공학박사 학위논문

A study on the thermal stability of water-soluble dyes and their application on ink-jet printed color filters

수용성 염료의 열안정성과 이를 이용한 잉크젯 프린트 컬러필터의 응용에 대한 연구

2013 년 2 월

서울대학교 대학원

재료공학부

김 영 도

Abstract

A study on the thermal stability of water-soluble dyes and their application on ink-jet printed color filters

Kim Young Do

Department of Materials Science and Engineering

The Graduate School

Seoul National University

While color filters produced by pigment-dispersed method have good thermal and photo-chemical stability, they have low chromatic properties due to the aggregation behavior of pigment particles used as colorants. Dyes can be attractive alternatives to overcome this limitation due to the reduced light scattering resulting from the fact that they are dissolved in the media and exist in molecular form. Although dyes have superior spectral characteristics, they are not widely used as coloring materials for liquid crystal display color filters owing to their low thermal stability. In this study, several perylene and phthalocyanine derivatives having high thermal stability were synthesized and then used to fabricate color filters by a spin-coating technique. The spectral and thermal stabilities of the color filters were investigated in comparison with those of pigment-dispersed color filters. The transmittance and color properties of the prepared color filters were higher and the thermal stability was similar to those of the pigment-dispersed color filters.

In order to manufacture a simple process of LCD color filters, ink-jet printed color filters were introduced using the synthesized RGB water-soluble dyes. Even though its chromaticity was unsatisfied due to their lower pattern thickness, the prepared dyes could be successfully applied to ink-jet printed LCD color filters since the thermal stability of ink-jet printed color filters was similar to that of spin-coated color filters.

Experimental studies on thermal stability of the water-soluble dyes were also conducted. For the investigation of structure–thermal stability relationships and thermal decomposition mechanism of water-soluble dyes, a series of structurally isomeric water-soluble azo naphthalene dyes were synthesized, and dye-based red color filters were fabricated using the synthesized azo dyes. Superior transmittance (98.9%) at 650 nm and a wide color gamut (62.8%) were achieved using one of the color filters. Thermal properties of the prepared isomeric dyes were examined by thermogravimetric analysis and differential scanning calorimetry. All the prepared isomeric azo dyes had a degradation temperature above 280 ^{o}C, varied with the dye structure. The degradation temperatures of the dyes were presumed to be related to the intra- and inter-molecular interactions of the structural isomers. It is confirmed that their intra-molecular interactions were similar from quantum mechanics calculations. However, the degradation temperatures generally increased as the proportion of their density. According to the molecular mechanics calculations, the structural differences gave rise to change of electrostatic attraction, steric hindrance and linearity of the dyes, which in turn caused changes in their molecular packing geometry, density and degradation temperature.

Thermal decomposition mechanism of the water-soluble dyes was also discussed. In case of the prepared isomeric azo dyes with strong electrostatic inter-molecular interactions decomposed gradually without melting and their degradation temperatures increased as the proportion of their

inter-molecular interaction. Thus, when the prepared water-soluble dyes had higher density – stronger inter-molecular interaction, they exhibited higher degradation temperatures since the dyes with stronger inter-molecular interactions could have stabilized intra-molecular interactions of the dye molecules. And the aggregates with larger diameters and higher aggregation numbers, would have stronger inter-molecular interaction and greater stabilized intra-molecular interactions than those with smaller particle sizes. This result could explain that, for the prepared water-soluble dyes, dye aggregates with smaller particle size degraded first and those with larger particle size degraded later.

KEYWORDS: LCD, Color filter, Pigment dispersed method, Ink-jet printing method, Transmittance, Chromaticity, Color gamut, Water-soluble dye, Thermal stability, Thermal decomposition, Azo dye, Perylene dye, Phthalocyanine dye, Intra-molecular interaction, Inter-molecular interaction

Student Number: 2003-21066

Contents

Chapter 1. Introduction

Chapter 2. The synthesis and application of thermally stable dyes for ink-jet printed LCD color filters

List of Tables

List of Schemes

List of Figures

Figure 2.4 CIE 1931 chromaticity diagram of NTSC (solid line), pigment-based color filter (dashed line), dye-based color filter using spin-coating (dotted line) and dye-based color filter using ink-jet printing (dash-dotted line).

Figure 2.5 FE-SEM images of color filters. (a) pigment-based color filter with pigment-crystalline particles. (b) dye-based color filter with dye aggregates.

Figure 2.6 Thermogravimetric analysis (TGA) of prepared dyes.

Figure 3.1 Reagents and representative synthetic scheme for the dyes studied.

Figure 3.2 Structures of the prepared dyes.

Figure 3.3 Spectral properties of the prepared color filters. (a) Absorption spectra of the fabricated color filters with 1 wt% of the prepared dyes. (b) Transmittance spectra of the fabricated color filters with 1 wt% of the prepared dyes. (c) Transmittance spectra of the color compensated red color filters with yellow dyes.

Figure 3.4 CIE 1931 chromaticity diagram of the prepared dye-based color filter (solid line) and previous dye-based color filter (dashed line).

Figure 3.5 TGA and density data. (a) TGA curves, degradation temperatures and densities of the prepared dyes, (b) The relationship between degradation temperature and density. (The weight

loss up to 150 ^{o}C is due to the evaporation of H_2O and DMF.)

Figure 3.6 The optimized molecular structure of **4a** (a) and **4b** (b) dyes by QM calculation. (unit =Å).

Figure 3.7 The representative packing structure of dye **4b** by MM calculation.

Figure 3.8 The optimized packing geometries of the dyes **1b**-**4b** by MM calculation.

Figure 4.1 TGA, DSC and density data of prepared dyes. (The weight loss up to 150 ^{o}C is due to the evaporation of H_2O and DMF.)

Figure 4.2 XRD data of dyes **4a** and **4b**.

Figure 4.3 Particle size analysis data of dyes **4a** and **4b.**

Figure 4.4 Two different decomposition mechanisms of dye molecules.

Figure 4.5 The representative UV-Vis absorption spectra and images of color change of water-insoluble dye (a) in cyclohexanone and dyes **1a** (b) and **4b** (c) in H_2O at the various temperatures.

Figure 4.6 Intra-molecular interaction of aggregates of the dyes **4a** and **4b**.

Chapter 1

Introduction

1.1 An overview of LCDs (Liquid Crystal Displays)

In the age of information, the display of information has become increasingly essential in many ways of everyday life. There exist several types of display system to visualize information such as cathode ray tubes (CRTs), electroluminescence (EL) devices, field emission devices (FEDs), plasma display panels (PDPs) and liquid crystal displays (LCDs). Each of displays has its own special characteristics and the proper choice of the display for a particular use, depends on many factors such as cost, size, brightness, definition, life, power consumption, temperature range, operating voltage and device circuit, etc. [1,2].

Among these display systems, the LCDs have emerged as the most promising displays during last decade. The extremely low power consumption, low voltage operation, high definition, compactness and flexibility of size are just some of the distinctive features which make LCDs preferable over other types of displays [3,4]. Figure 1.1 shows a basic structure of LCD panel. The LCD is basically consisted of a thin layer of liquid crystal sandwiched between a pair of polarizers. To control the optical transmission of the display element electronically, the liquid crystal layer is placed between transparent electrodes [e.g., indium tin oxide (ITO)]. The polarizer and the electrodes are cemented on the surfaces of the glass plates. A minimum thickness of a few millimeters is needed to maintain the structural integrity of the panel. The thickness of the liquid crystal layer is kept uniform by using spacers that are made of photosensitive polymers. By applying a voltage across the electrodes,

an electric field inside the liquid crystal can be obtained to control the transmission of light through the liquid crystal cell. To achieve the display of information, we need a two-dimensional array of these electrodes. These electrodes can be electrically driven for data input by using two sets (x,y) of parallel array of electrodes. Color filter (CF) is a key component for rendering color images in LCD panel. The color filter layer is fabricated with colorants of red (R), green (G), and blue (B) from either dyes or pigments. These colorants convert white backlight into R, G, B colors

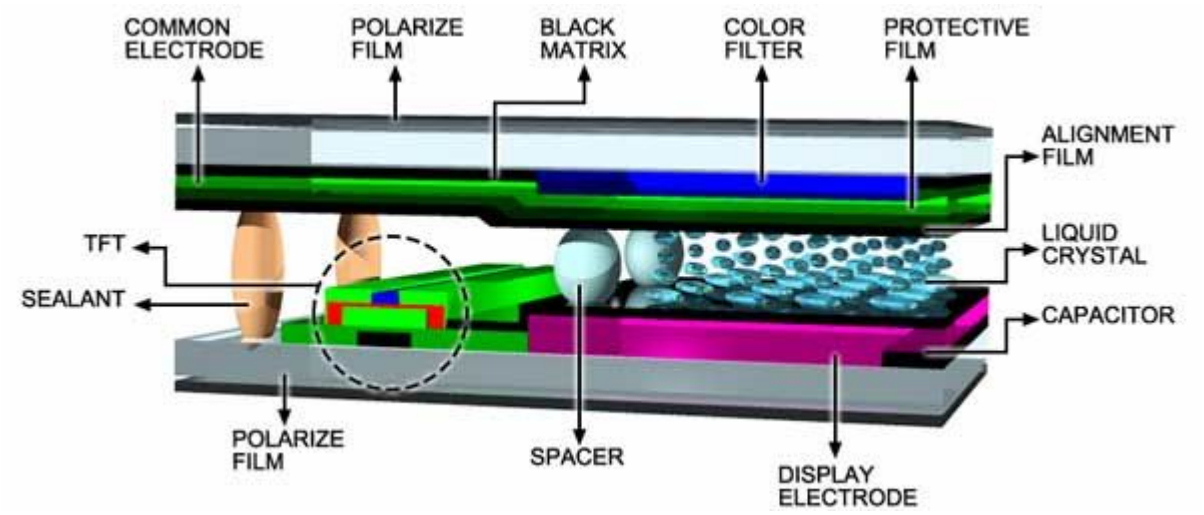

Figure 1.1 Basic structure of Liquid crystal display (LCD).

1. 2 Structure of LCD Color Filters (CFs)

The fundamental structure of LCD color filters is magnified in Figure 1.2 [3,4]. A color filter consists of clear substrate, black matrix (BM), color filter layer (RGB colors), overcoat layer, and column spacer. The clear substrate is generally used by thin glass or plastic. The black matrix material is coated on clear substrate in the optically inactive areas to prevent light leakage and provide a light shield for the amorphous silicon transistors. The black matrix material should have a low reflectance to optimize contrast ratio (CR). Black matrix material can be used by organic or inorganic, with carbon black a most popular organic choice. The RGB colors are fabricated which contain red, green and blue colors from either dyes or pigments. After the color layer is formed, protection overcoat layer is deposited. Transparent acryl resin, polyimide resin or polyurethane resin are used for overcoat material. The purpose of overcoat layer is the reduction of color pattern's thickness variation, durability against sputtering and chemical resistance. Especially, the overcoat layer is important for dyeing CF and printing CF. For the dyeing CF, the overcoat layer is necessary to protect the liquid crystal from impurities in the CF layer and to increase the chemical stability. In printing CF, the overcoat layer flattens the CF surface. A column spacer is a material used to maintain a uniform cell gap between the TFT and the color filter glass. There are two kinds of spacer applied in LCD panel, a bead spacer and a photo-spacer. A bead spacer is not adequate for larger-sized LCD panels because of the low uniformity of the cell gap and many problems in manufacturing process. For this reason, bead spacers are being changed to photo-spacers to satisfy today's manufacturing trend. A photo-spacer is patterned on the color filter glass, exactly on the blue pattern, by using a negative photo-resist, and the process includes cleaning, coating, exposure, developing and oven baking.

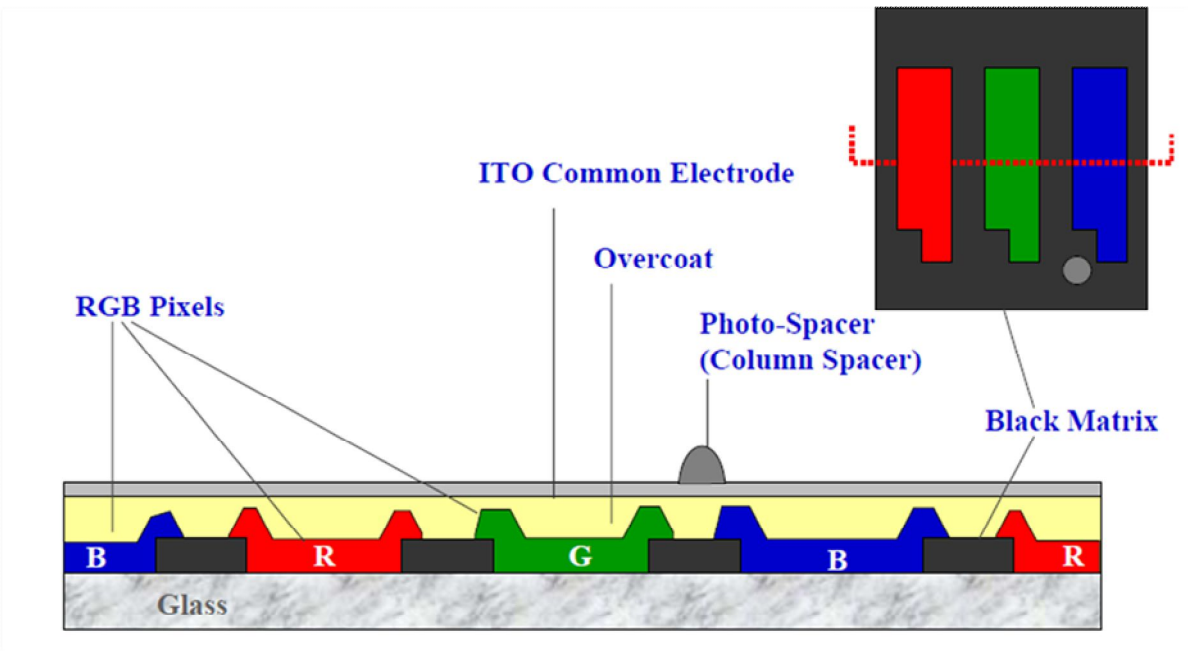

Figure 1.2 Fundamental structure of LCD color filters.

1. 3 Requirements of color filters

1.3.1 High color purity and high transmittance

This property is essential for good color representation. In order to have both high quality color picture and brightness in TV, notebook PC and monitor, the LCD panel is required to have high color purity and high transmittance. Therefore, the selection of the colorants such as pigments and dyes should be based on sharp spectrum eliminating unnecessary wavelengths and retaining only the necessary light [6-8]. Besides, the surface roughness of colored patterns caused by pigments can affect the color characteristics of the filter. The roughness is produced by the pigment particles lying on the surface of the coloring layer. The surface of a colored pattern becomes cloudy and thereby decreases the transmittance [10,11]. This drawback can be controlled by adding leveling agent or optimizing conditions of manufacturing process such as soft-bake and development.

1.3.2 High contrast

The color filter contrast is defined as the ratio of transmissive light intensity of setting two polarizer parallel to intensity of setting them across, setting the color filter between two polarizer sheet. High contrast characteristic is necessary for high color purity and good legibility [9]. The depolarization effect is the most important optical characteristics of the color filter. It occurs when the light that is linearly polarized by passing through a polarizer plate is distributed in the film due to the scattering and birefringence by pigment particles. It causes a reduction in the contrast ratio. The low contrast ratio of the film may cause a serious problem with active matrix liquid crystal displays (AMLCD). This problem can be overcome

by decreasing the particle size and improving the stability of dispersion.

1.3.3 Low reflection

Reflectivity of TFT-LCD module is mainly determined by black matrix material on color filter. Chromium, chrome oxide or black resins have been widely used for STN-LCD and TFT-LCD because of light shielding ability and low reflection. High resistivity, high optical density (OD), high light shielding, high resolution, low reflectance and low cost black matrix is preferred for LCD applications.

1.3.4 High stability against heat, light and chemical

The color filters must exhibit high heat resistance without thermal flow and chromatic changes during the alignment layer formation step. The chromatic changes (ΔE_{ab}) should be less than 3 after heating at 250^{o}C for 1 h [10,11]. The light stability of the pixels is important because these pixels are illuminated with back light of LCDs. The CFs are exposed to a mercury–xenon lamp with ultraviolet (UV) filter for more than two million lux hours. The chromatic changes (ΔE_{ab}) after exposure should be less than 3 [4,5]. The chemical stability is a key factor since CFs are exposed to solvents, acids and bases during the LCD fabrication process. The cured film must be resistant towards alignment layer solvents such as NMP and γ-butyrolactone, towards acids during etching of the ITO or towards bases used in the development system [4,5].

1.4 Fabrication of RGB color pattern using Color Photo-resist (Color PR, CPR)

1.4.1 Color Photo-resist (Color PR, CPR)

A photo-resist is a light-sensitive material used in several industrial processes, such as photolithography and photoengraving to form a patterned coating on a surface. Photo-resists are classified into two groups: positive and negative-tone resists.

- A *positive-tone photo-resist* is a type of photo-resist in which the portion of the photo-resist that is exposed to light becomes soluble to the photo-resist developer. The portion of the photo-resist that is unexposed remains insoluble to the photo-resist developer.
- A *negative-tone photo-resist* is a type of photo-resist in which the portion of the photo-resist that is exposed to light becomes insoluble to the photo-resist developer. The unexposed portion of the photo-resist is dissolved by the photo-resist developer.

The color photo-resist is negative-tone photo-resist which is made up of coloring material, dispersant, photo-sensitive binder, multi-functional monomer, photo-initiator and additives such as leveling agent and coupling agent as shown in Figure 1.3.

An acryl-based photo-polymerizable material is used as binder system materials since the acryl polymer has a superior transparency. The binders have influence on heat light stability, coating flatness, adhesion to substrate, hardness, developability and durability. Since pigments have strong absorption in i-, h-, and g-line region, by fixing multi-functional monomers and photo-initiators, the materials with higher photosensitivity can be made.

Colorant system is consisted of pigment and dispersant which is pigment-derivative dispersant. In particular, considering of spectral property, chromaticity and stability, the

colorants are limited to eleven pigments as shown in Table 1.1.

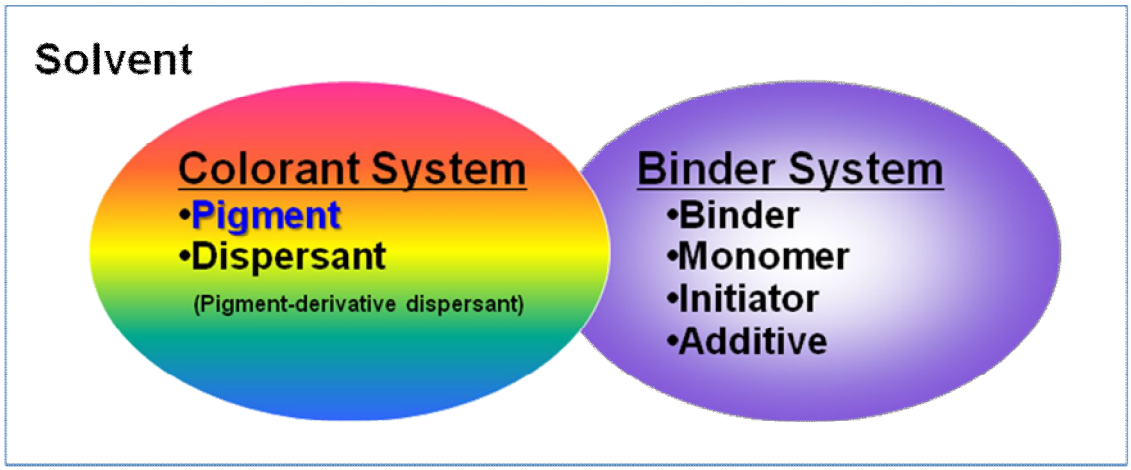

Figure 1.3 Components of color photo-resist.

Table 1.1 Conventional colorants for LCD color filters.

Color	Color Index Number	Structure
Red	C.I. Pigment Red 177	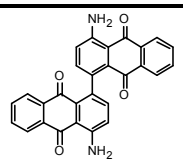
	C.I. Pigment Red 254	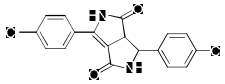
Green	C.I. Pigment Green 7	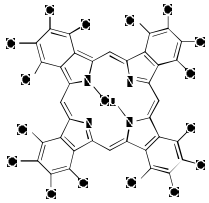
	C.I. Pigment Green 36	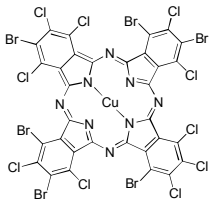
	C.I. Pigment Green 58	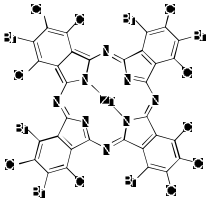
Blue	C.I. Pigment Blue 15:6	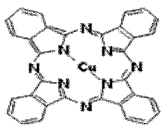
	C.I. Pigment Blue 60	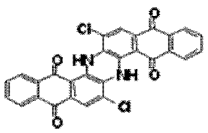
Violet	C.I. Pigment Violet 23	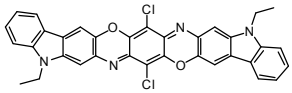
Yellow	C.I. Pigment Yellow 138	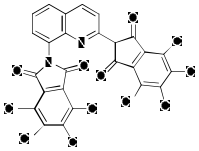
	C.I. Pigment Yellow 139	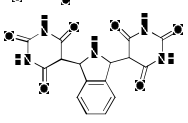
	C.I. Pigment Yellow 150	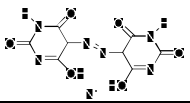

1.4.2 Fabrication of RGB color pattern

Conventional fabrication process of color filters is following complicated photolithographic method using color photo-resist [4,5] as shown in Figure 1.4.

1. Black matrix formation;

   A black matrix is formed first in order to prevent any leakage of backlight and the RGB color mixture.

2. Color resist coating;

   Color photo-resist is coated on the entire glass substrate surface.gjjgj

3. Exposure;

   To make the pattern insoluble, it is UV cured by exposure through a photo-mask.

4. Development & baking;

   After the removal of unnecessary portions of the color resist by the developing solution, the pattern is cured through baking.

2-4. Repeat of step 2 to 4;

   The above processes from step 2 to 4 are repeated three times (for RGB).

5. ITO film formation;

   ITO film (transparent conductive film) is formed by the spattering method.

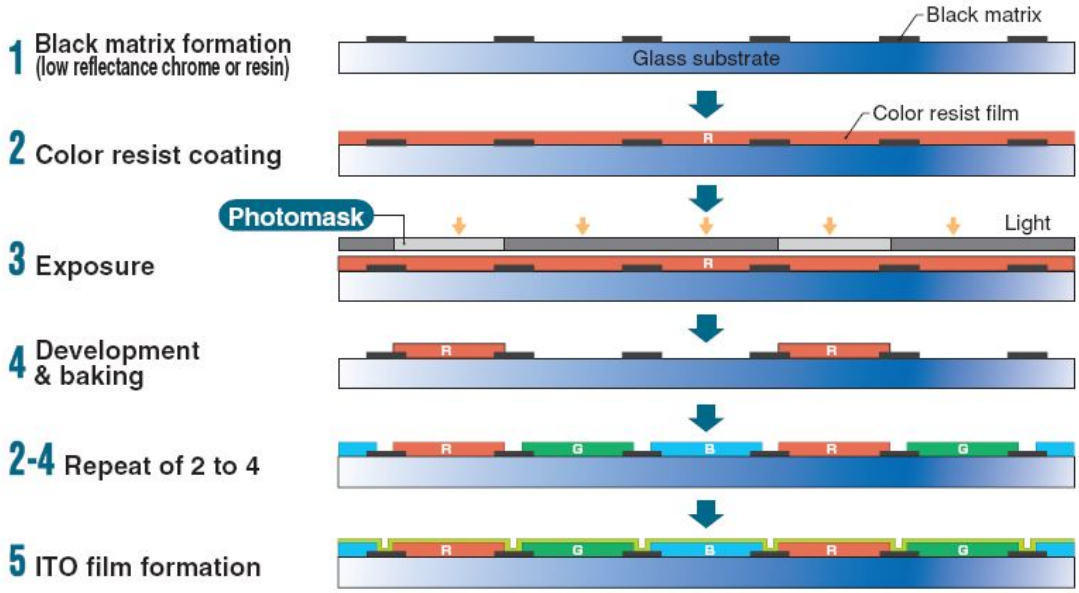

Figure 1.4 Color filter manufacturing process by the photolithographic method.

1.5 Classification of colorants

Colorants can be classified into two main groups: *pigments* and *dyes*. Figure 1.5 shows schematic diagram of classification between *pigments* and *dyes*. When inter-molecular interaction of colorant molecules (F_{mm}) is stronger than interaction between colorant molecule and solvent (F_{ms}), the coloring materials would exist as crystalline particles (aggregates or agglomerates), which results in high stability for heat, light and chemical. And they are insoluble in media solvent but dispersed with surfactant. Therefore, they would decrease transmittance of color filters. This colorant belongs to the group of *pigments*.

In case of *dyes*, on the other hand, when F_{ms} is stronger than F_{mm}, the colorants would dissolve in media (organic solvent or water) and behave as a molecule, resulting in reducing of light scattering. Therefore, the *dyes* have superior optical properties such as transmittance and color strength although they have lower stability than *pigments*. A *solvent dye* is a dye soluble in organic solvents. It is usually used as a solution in an organic solvent. However, *water-soluble dyes* are very polar and ionized in water - they are salt-like materials and they could have stronger inter-molecular interaction than solvent dyes owing to the electrostatic interactions such as ionic interaction and dipole-dipole/dipole-induced dipole inter action.

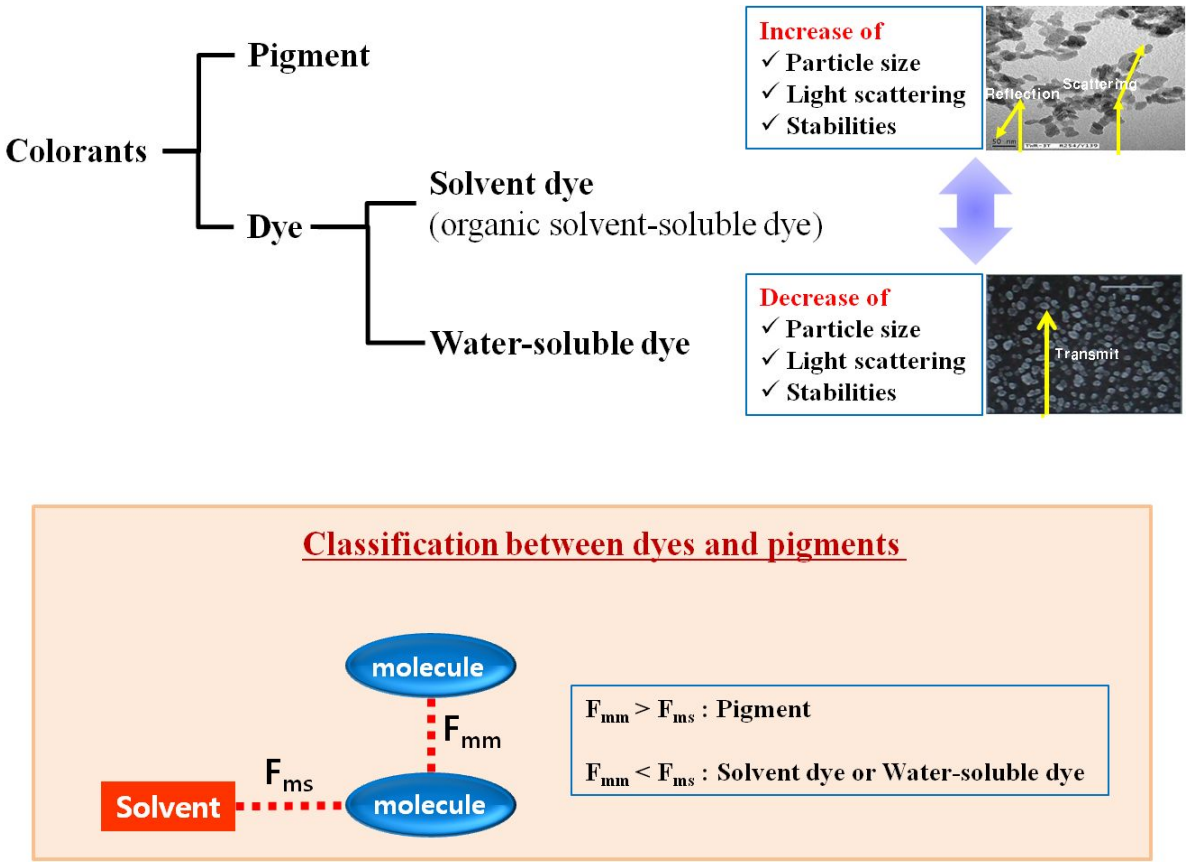

Figure 1.5 Schematic diagram of classification between pigments and dyes.

1.6 Previous researches

In case of LCD devices, only 5-7 % of the backlight can pass through the whole panel, which includes a polarizing filter, TFT-array, LC cell, and color filter. In particular, the transmittance through the color filter is the lowest (25-30%). Therefore, developing high transmittance color filters is essential for saving energy consumption as well as improving high-quality displays. In order to improve transmittance of the color filters, over the past few decades, a considerable number of studies have been conducted on minimizing of particle size of pigment. However, color filters produced by pigment-dispersed method have a limitation - low chromatic property due to the aggregation behavior of pigment particles used as colorants. Therefore, dyes could be attractive alternatives to overcome this limitation due to the reduced light scattering resulting from the fact that they are dissolved in the media and exist in molecular form. Nevertheless, in order for the dyes to be applied successfully to the LCD manufacturing process, their low thermal stability needs to be improved. Moreover, they should be highly soluble in industrial solvents and have sharp absorption peaks for superior optical properties.

In our research group (Prof. J.P. Kim group), organic solvent-soluble red perylene dyes were synthesized for LCD color filters. Perylene-3,4,9,10-tetracarboxylic diimide derivatives show excellent thermal stability originating from their very high resonance stabilization energy and π-π interactions due to the planar molecular structure. In addition, they have very strong and sharp absorption at approximately 530 nm. However, they have low solubility in common industrial solvents, such as cyclohexanone, which limits their applications [10].

Our research group was also prepared dye-based green color filters using phthalocyanine and benzoperylene dyes (solvent dye), which was the first report of applying 100% dyes to

the green color resist for photolithography process. The green color, which transmits light within the range of 520–550 nm, has the greatest contribution to the optical property of color filters since it is the most sensitive to human eyes [3].

1.7 Research Purpose

Current fabrication method for LCD color filters is photolithography using pigments as coloring materials. However, it has some disadvantages such as the complicated process, waste of photo-resist and low optical property of color filters. And, with the progress of display, needs of using water-soluble dyes in this industry for the environmentally friendly organic solvent-free coloring process has increased. Therefore, the paradigm of materials and manufacturing process should be changed in organic solvent-free materials and direct printing method such as roll-to-roll and ink-jet printing [12-16]. In this study, water-soluble dyes and ink-jet printed color filters would be introduced. That is, according to the shift of pigment to water-soluble dyes, optical property such as transmittance can be enhanced, and color filters would be manufactured in eco-friendly environment. Also, complicated fabrication process of color filters can be simplified by ink-jet printing method.

On the other hand, there have been few systematic investigations of the thermal stability of water-soluble dyes for these purposes. Therefore, in this study, academic investigation of structure–thermal stability relationships and thermal decomposition mechanism of water-soluble dyes will be discussed.

The following contexts consist of three parts:

Chapter 2 The synthesis and application of thermally stable dyes for ink-jet printed LCD color filters

Chapter 3 Synthesis, application and investigation of structure–thermal stability relationships of thermally stable water-soluble azo naphthalene dyes for LCD red color filters

Chapter 4 A study on thermal decomposition behavior of some water-soluble azo dyes

1.8 References

[1] Yeh P, Gu C. Optics of liquid crystal displays. John Wiley & Sons, Inc; 1999. P. 1-5.

[2] Yang DK, Wu ST. Fundamentals of liquid crystal devices. New Jersey: Wiley-SID; 2006 p. 278–281.

[3] Choi J, Kim SH, Lee WS, Yoon C, Kim JP. Synthesis and characterization of thermally stable dyes with improved optical properties for dye-based LCD color filters. New J. Chem. 2012; 36:812–818.

[4] Sabnis RW. Color filter technology for liquid crystal displays. Displays 1999;20:119–29.

[5] Tsuda K. Color filters for LCDs. Displays 1993;14:115–124.

[6] Yeh P, Gu C. Optics of liquid crystal displays. New York: John Wiley & Sons, Inc.; 1999 p. 270–272.

[7] Sugiura T. Dyed color filters for liquid-crystal displays. Journal of the SID 1993;1:177–180.

[8] Kim YD, Kim JP, Kwon OS, Cho IH. The synthesis and application of thermally stable dyes for ink-jet printed LCD color filters. Dyes and Pigments 2009;81:45–52.

[9] Yeh P, Gu C. Optics of liquid crystal displays. New York: John Wiley & Sons, Inc.; 1999 p. 198–222.

[10] Choi J, Sakong C, Choi JH, Yoon C, Kim JP. Synthesis and characterization of some perylene dyes for dye-based LCD color filters. Dyes and Pigments 2011;90:82–88.

[11] Sakong C, Kim YD, Choi JH, Yoon C, Kim JP. The synthesis of thermally-stable red dyes for LCD color filters and analysis of their aggregation and spectral properties. Dyes and Pigments 2011;88:166–173.

[12] Chang CJ, Chang SJ, Shin KC, Pan FL. Improving mechanical properties and chemical

resistance of ink-jet printer color filter by using diblock polymeric dispersants. Journal of Polymer Science: Part B: Polymer Physics 2005;43:3337−3353.

[13] Koo HS, Chen M, Pan PC, Chou LT, Wu FM, Chang SJ, Kawai T. Fabrication and chromatic characteristics of the greenish LCD colour-filter layer with nano-particle ink using inkjet printing technique. Displays 2006;27;124–129.

[14] Koo HS, Chen M, Pan PC. LCD-based color filter films fabricated by pigment-based colorant photo resist inks and printing technology. Thin Solid Films 2006;515;896–901.

[15] Ohya H, Morimoto H. Water based ink composition and image forming method. US 2001/0023652 A1.

[16] Kim YD, Cho JH, Park CR, Choi JH, Yoon C, Kim JP. Synthesis, application and investigation of structure–thermal stability relationships of thermally stable water-soluble azo naphthalene dyes for LCD red color filters. Dyes and Pigments 2011;89:1-8.

Chapter 2

The synthesis and application of thermally stable dyes for ink-jet printed LCD color filters

2.1 Introduction

Color filter (CF) is a key component for rendering color images in liquid crystal displays (LCD) panel. The color filter layer is fabricated with colorants of red (R), green (G), and blue (B) from either dyes or pigments. These colorants convert white backlight into R, G, B colors [1-2].

In manufacturing CFs, there are four traditional processes, which include dyeing, pigment dispersion, printing and electrodeposition method [3-4]. Among these technologies, the pigment dispersion method has been widely used in mass production of CF for LCD since it can produce CFs of high durability and good color reproducibility. However, this method has spectral drawbacks such as decreased transmittance of light and contrast ratio caused by aggregation of pigment particles [5].

In order to manufacture LCD panels of higher resolution and larger-size, some innovative methods for CF have been tried such as ink-jet printing, latent pigment technology and acid proliferation type pigment dispersion [6-10]. Among these technologies, researches on ink-jet printing method are active nowadays, thanks to the full development of digital printing technology. However, all these approaches use pigments, therefore they have the aforementioned limitation of transmittance and contrast ratio.

On the other hand, dye-based CF (D-CF) can have higher transmittance and contrast ratio due to lower light scattering since dyes can be dissolved in a media and exist in molecular phase. Especially, for the ink-jet system which needs highly concentrated ink, the dye-based ink is more suitable than pigment-based ink. Thus, to overcome the limited optical performance of CF with pigments, applying dyes to CF can be an attractive alternative.

It was previously studied that CF fabricated by dyeing method was characterized by high transmittance and good color purity. However, the dyeing method using dyes as coloring materials is not widely used for commercial manufacturing process of CF due to the unsatisfactory thermal, light and chemical resistance of dyes [11]. Thermal stability of dyes is a main drawback while light and chemical stability are not so serious problems. In case of photo-stability, the light emitted from the backlight unit loses considerable energy as it passes through first polarizing film, glass, TFT array and liquid crystal. Also, the light entered from outside is blocked by frontal anti UV-coating film, second polarizing film, indium tin oxide (ITO) and overcoat layer, thereby preventing photo-fading of the colorants [12,13]. Moreover, the photo-fading can be decreased by mixing auxiliaries such as antioxidants containing benzophenone moiety [14,15]. The chemical stability of colorants can also be compensated by the overcoat layer. However, many dyes are not as resistant to heat as pigments. Discoloration of dye easily occurs during the alignment layer forming step performed at 230 oC for an hour. Thus, it is indispensable to improve thermal stability of dyes for commercial production of dye-based CF.

In this study, we have designed and synthesized perylene and phthalocyanine based dyes of high thermal stability and superior spectral property for ink-jet printed CF. The structure of the dyes are designed so that they can induce sufficient intermolecular packing. In addition, the dyes are designed to have high water solubility so that they can be dissolved into the main media of the ink i.e. water. With the synthesized dyes, CF was fabricated via direct ink-jet

printing on the black matrix patterned glass. The heat-resistance, transmittance and color gamut of the prepared CF were investigated and compared with those of pigment-based CF.

2.2 Experimental

2.2.1 Materials and instrumentation

3,4,9,10-Perylene-tetracarboxylic dianhydride, 4-chloroaniline, 4-bromoaniline, sulfanilic acid, m-cresol, fuming sulfuric acid (oleum) of 20 % SO_3 from Sigma-Aldrich, and 6-amino-2-naphthalene-sulfonic acid, isoquinoline, Co-phthalocyanine, Cu-phthalocyanine, Ni-phthalocyanine, Zn-phthalocyanine, 2,4-dinitro-1-naphthol-7-sulfonic acid disodium salt (C.I. Acid Yellow 1), C.I. Acid Violet 43 from TCI were used. ORASOL® Yellow 4GN (C.I. Solvent Yellow 146) was supplied by Ciba Korea Ltd. Pigment-based color resists of NF-R017D (red), NF-G022M (green), NF-B016M (blue) were supplied by Dongwoo Fine-Chem. All other reagents and solvent were reagent-grade quality and obtained from commercial suppliers. Transparent glass substrate was provided from Paul Marienfeld GmbH & Co. KG.. Commercial acrylic binders of LM100, LM300, LM500 and Cr-based black matrix patterned glass were supplied by LG Micron Co., Ltd.

^{1}H-NMR spectra were recorded by Bruker Avance 500 at 500MHz using DMSO-d_6, as solvent and TMS as the internal standard. Fourier transform infrared (FT-IR) spectra were recorded as KBr pellets on a Perkin Elmer Spectrum 2000 FT-IR spectrometer. Matrix Assisted Laser Desorption/Ionization Time Of Flight (MALDI-TOF) mass spectra were collected on a Voyager-DE STR Biospectrometry Workstation with α-cyano-4-hydroxy-cynamic acid (CHCA) as matrix. Absorption and transmittance spectra were measured on a

HP8452A spectrophotometer. Chromatic characteristics of CFs were analyzed by Otsuka Electronics LCF A2000 spectrometer. Thickness of the CFs was measured using Nano System Nanoview E-1000. Thermogravimetric analysis (TGA) was conducted under nitrogen at a heating rate 10K/min with a TA Instruments Thermogravimetric Analyzer 2050.

2.2.2 Synthesis

2.2.2.1 Synthesis of dye intermediates (1a-d)

N,N'-bis-(4-chlorophenyl)-3,4,9,10-perylenebis(dicarboximide) (**1a**) was prepared according to the following procedure. A mixture of 3,4,9,10-perylene-tetracarboxylic dianhydride (19.6 g, 0.05 mol), 4-chloroaniline (12.8 g, 0.1 mol), m-cresol (300 ml) and isoquinoline (30 ml) was stirred at 50 ^{o}C for 2 hour. The solution was heated at 130 ^{o}C for 5 hours, the temperature was raised to 150 ^{o}C and kept for 4 hours. The reaction was then completed by stirring at 200 ^{o}C overnight. The warm solution was poured into 250 ml of acetone, and the precipitate was filtered out and dried at 100 ^{o}C under vacuum. The crude product was washed with 5 % NaOH until the characteristic green fluorescent color of perylene dianhydride disappear and the unreacted 4-chloroaniline and high boiling point solvents, m-cresol and isoquinoline were cleared by ethanol reflux for 2 hours. Dyes of **1b-d** were synthesized in the same manner with dye **1a** using 4-bromoanilene, sulfanilic acid and 6-amino-2-naphthalene-sulfonic acid (Scheme 2.1). The yields, ^{1}H-NMR, FT-IR and Mass data of the dyes are given below.

(**1a**): yield 83.2 %; ^{1}H-NMR (DMSO-d_6, ppm): 9.12 (d, 4H), 8.65 (d, 4H), 7.62 (d, 4H), 7.50 (d, 4H); FT-IR (KBr, cm^{-1}): 1705 (C=O), 1356 (C–N); MALDI-TOF MS: *m/z* 649.94 (100%,

$[M+K]^+$).

(**1b**): yield 81.5 %; ^{1}H-NMR (DMSO-d_6, ppm): 9.00 (d, 4H), 8.60 (d, 4H), 7.55 (d, 4H), 7.44 (d, 4H); FT-IR (KBr, cm^{-1}): 1703 (C=O), 1357 (C–N); MALDI-TOF MS: *m/z* 685.38 (100%, M^+).

(**1c**): yield 75.7 %; ^{1}H-NMR (DMSO-d_6, ppm): 8.62 (d, 4H), 8.53 (d, 4H), 8.25 (d, 4H), 8.20 (d, 4H); FT-IR (KBr, cm^{-1}): 1700 (C=O), 1358 (C–N), 1255, 1181 (S=O), 642 (S–O); MALDI-TOF MS: *m/z* 746.90 (100%, $[M+2Na]^+$).

(**1d**): yield 77.8 %; ^{1}H-NMR (DMSO-d_6, ppm): 8.42 (s, 2H), 8.07 (d, 4H), 7.82 (d, 4H), 7.67 (d, 2H), 7.58 (d, 2H), 7.35 (d, 2H), 7.16 (s, 2H), 7.10 (d, 2H); FT-IR (KBr, cm^{-1}): 1704 (C=O), 1348 (C–N), 1200, 1096 (S=O), 615 (S–O); MALDI-TOF MS: *m/z* 824.78 (100%, $[M+Na]^+$).

2.2.2.2 Synthesis of 1,7-disulfo-3,4,9,10-perylenebis(dicarboximide) derivatives (2a-d)

Since the synthetic procedures of perylene dyes **2a-d** are all similar, only **2a** is given as a representative example (Scheme 2.1). 6g (0.01 mol) of N,N'-bis-(4-chlorophenyl)-3,4,9,10-perylenebis(dicarboximide) (**1a**) with 30 ml of oleum (20% SO_3) was refluxed at 145 ^oC for 6 hours under Ar atmosphere. The hot solution was cooled at room temperature and dropwised into 200 ml of N,N-dimethylmethanamide. Then, the mixture solution was poured into 1400 ml of acetone, and the precipitate of **2a** was filtered out and dried at 40 ^oC under vacuum. In order to remove the remaining sulfuric acid, the product was dissolved in 800 ml of distilled water. After addition of sodium chloride (50 g) to the solution, the precipitate formed was filtered, washed with ethanol and dried in a vacuum oven at 40 ^oC. The purity of **2a** was confirmed by thin layer chromatography using isopropyl alcohol/acetone/ammonia

(1:2:1). The yields, ^{1}H-NMR, FT-IR and Mass data of the dyes are given below.

(**2a**): yield 68.8 %; ^{1}H-NMR (DMSO-d_6, ppm): 8.80 (d, 4H), 8.50 (d, 4H), 7.91 (s, 2H), 7.58 (d, 2H), 7.43 (d, 2H); FT-IR (KBr, cm^{-1}): 1701 (C=O), 1360 (C–N), 1233, 1069 (S=O), 625 (S–O); MALDI-TOF MS: *m/z* 772.05 (100%, $[M+2H]^+$).

(**2b**): yield 72.3 %; ^{1}H-NMR (DMSO-d_6, ppm): 8.73 (d, 4H), 8.45 (d, 4H), 7.94 (s, 2H), 7.76 (d, 2H), 7.33 (d, 2H); FT-IR (KBr, cm^{-1}): 1700 (C=O), 1358 (C–N), 1233, 1058 (S=O), 623 (S–O); MALDI-TOF MS: *m/z* 904.89 (100%, $[M+2Na]^+$).

(**2c**): yield 65.3 %; ^{1}H-NMR (DMSO-d_6, ppm): 8.90 (d, 4H), 8.67 (d, 4H), 7.79 (s, 2H), 7.74 (d, 2H), 7.53 (d, 2H); FT-IR (KBr, cm^{-1}): 1708 (C=O), 1328 (C–N), 1195, 1041 (S=O), 617 (S–O); MALDI-TOF MS: *m/z* 861.93 (100%, $[M+4H]^+$).

(**2d**): yield 71.2 %; ^{1}H-NMR (DMSO-d_6, ppm): 9.29 (s, 2H), 9.15 (s, 2H), 9.05 (d, 2H), 8.87 (d, 2H), 8.64 (d, 2H), 8.40 (d, 2H), 8.33 (d, 2H), 8.07 (s, 2H), 7.80 (d, 2H); FT-IR (KBr, cm^{-1}): 1709 (C=O), 1362 (C–N), 1193, 1041 (S=O), 615 (S–O); MALDI-TOF MS: *m/z* 961.98 (100%, $[M+4H]^+$).

2.2.2.3 Synthesis of sulfonated metal-phthalocyanine (3a-d)

Water soluble dyes with metal-phthalocyanine moiety (**3a-d**) were synthesized by heating metal phthalocyanines in oleum (Scheme 2.1). 5 g of metal-phthalocyanine with 20 ml of oleum (20 % SO_3) was refluxed at 145 ^{o}C for 3 hours. In the case of zinc-phthalocyanine, however, the mixture was stirred at 90 ^{o}C for 6 hours. The solution was added into 500 ml of distilled water. After addition of sodium chloride (80 g) to the solution, the precipitate formed was filtered, washed with ethanol and dried in a vacuum oven at 40 ^{o}C. The crude product was refluxed in ethanol for 2 hrs, hot filtered, washed with hot ethanol and subsequently dried in vacuum oven. The yields, FT-IR and Mass data of the dyes are given below.

(**3a**): yield 81.3 %; FT-IR (KBr, cm^{-1}): 1640 (C=N), 1422, 1145 (S=O), 622 (S–O); MALDI-TOF MS: *m/z* 892.58 (100%, $[M+4H]^+$).

(**3b**): yield 88.0 %; FT-IR (KBr, cm^{-1}): 1638 (C=N), 1396, 1141 (S=O), 622 (S–O); MALDI-TOF MS: *m/z* 896.70 (100%, $[M+4H]^+$).

(**3c**): yield 83.5 %; FT-IR (KBr, cm^{-1}): 1633 (C=N), 1331, 1193 (S=O), 637 (S–O); MALDI-TOF MS: *m/z* 891.84 (100%, $[M+4H]^+$).

(**3d**): yield 87.7 %; FT-IR (KBr, cm^{-1}): 1638 (C=N), 1326, 1192 (S=O), 658 (S–O); MALDI-TOF MS: *m/z* 898.86 (100%, $[M+4H]^+$).

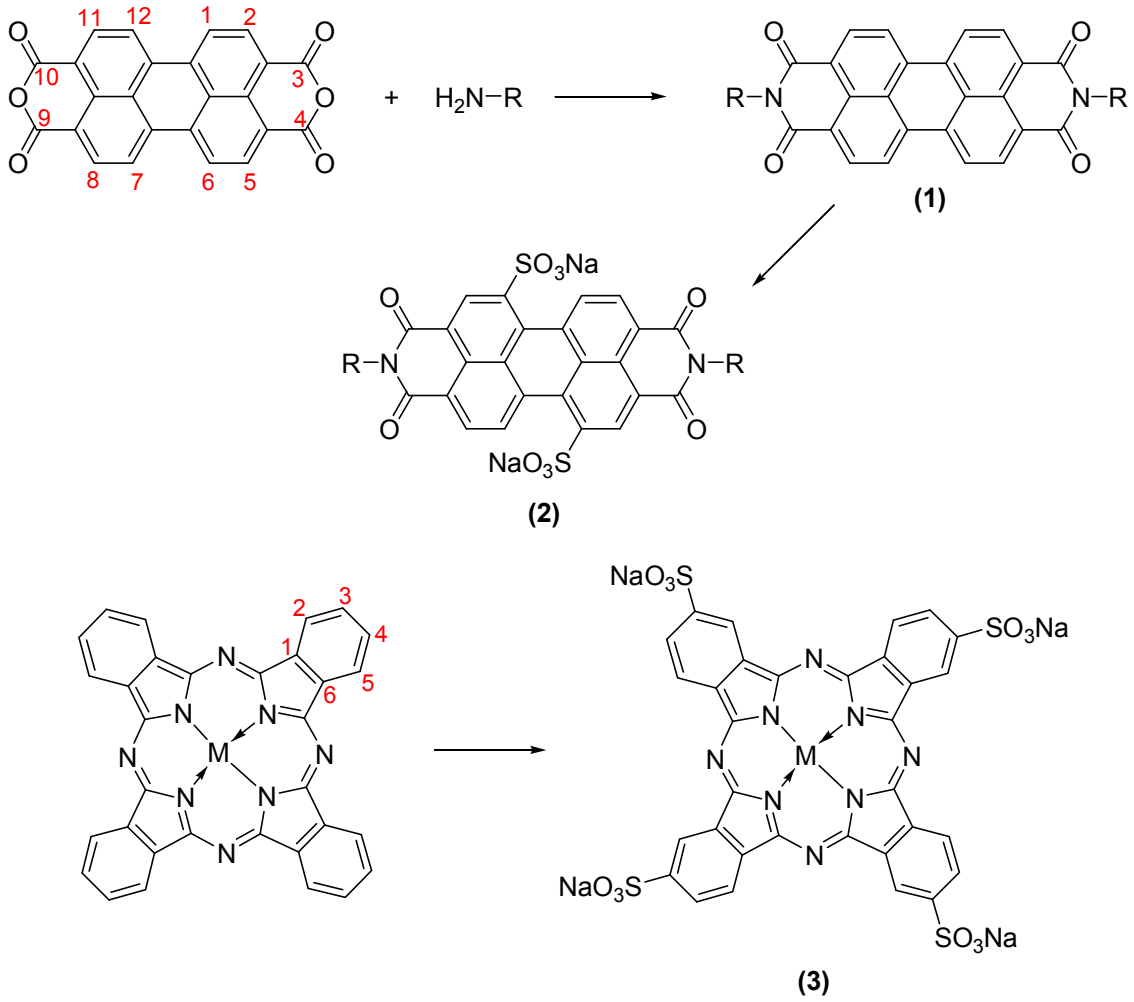

1, 2	R
a	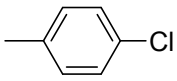
b	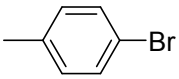
c	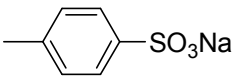
d	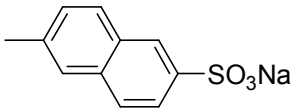

3	M
a	Co
b	Cu
c	Ni
d	Zn

Scheme 2.1 Synthesis of thermally stable dyes**.**

2.2.3 Preparation of dye-based inks

Aqueous red ink was composed of dye **2a** (1.0 g), C.I. Solvent Yellow 146 (0.5 g), distilled water (7.5 ml), N,N-dimethylmethanamide (2 ml) and LM100 (0.5 ml) as a binder based on acrylate. Aqueous green ink was prepared with dye **3d** (1.0 g), C.I. Acid Yellow 1 (0.5 g), distilled water (9.5 ml) and LM300 (0.5 ml). Aqueous blue ink was made up of dye **3b** (1.0 g), C.I. Acid Violet 43 (0.5 g), distilled water (9.5 ml) and LM500 (0.5 ml).

2.2.4 Fabrication of pigment-based and dye-based color filters

2.2.4.1 Fabrication of pigment-based CFs using spin-coating method

Commercial pigment-based inks were coated on transparent glass substrate using MIDAS System SPIN-1200D spin coater. The coating speed was kept for 5 seconds at 100 rpm. Then, the speed was raised up to 800 rpm and kept constant for 20 seconds. Wet pigment-coated CFs were baked at 180 ^{o}C for 1 hour. Thickness of them was around 1.7 μm.

2.2.4.2 Fabrication of dye-based CFs using spin-coating method

Prepared dye-based inks were coated on transparent glass substrate using MIDAS System SPIN-1200D spin coater. The coating speed was kept for 5 seconds at 100 rpm. Then, the speed was raised up to 700 rpm and kept constant for 20 seconds. On the other hand, dye-based red CF was coated at 100 rpm for 5 seconds and the coating speed was raised to 1500

rpm and kept constant for the same time. Wet dye-coated CFs were baked at 180 ^{o}C for 30 minutes, the temperature was raised to 220 ^{o}C and kept for 1 hour. All dye-based CFs through spin-coating had 1.7 μm of thickness.

2.2.4.3 Fabrication of dye-based CFs using ink-jet printing method

The Cr-based black matrix was fabricated as previously described [8,9]. To facilitate adherence of the colorant inks in the black matrix patterned glass of sub-pixels, the patterned glass was previously treated with plasma of CF_4 and O_2 using Korea Vacuum Tech. MEICP before printing [9]. The inks were printed using UJ 100 ink-jet printer made by UNIJET Co., Ltd. The size of nozzle was around 30 μm. After printing, these inks were heated at 180 ^{o}C for 30 minutes, the temperature was raised to 220 ^{o}C and kept constant for 1 hour. The dimension of one sub-pixel cell is around 27 μm by 88.0 μm by 1.2 μm which can contain 32.1 to 42.8. pico liter of ink, and the thickness of each colorant film in the cell will be 0.8 μm.

2.2.5 Investigation of spectral and chromatic properties

Transmittance spectra of pigment-based CFs and dye-based CFs were examined by UV-vis. spectrophotometer. Chromatic properties of them were investigated by color spectrophotometer (LCF A2000). In case of ink-jet printed CFs, monitoring with a CCD camera of LCF A2000, the transmittance and chromaticity of separated sub-pixels on the substrates could be measured.

2.2.6 Investigation of thermal stability

2.2.6.1 Thermal stability of synthesized dyes

Thermogravimetric analysis was used to examine decomposition temperature and relative weight losses of synthesized dyes. The prepared dyes were heated to 110 ^{o}C for 10 minutes to remove any residual water and solvent. Then, it was heated to 220 ^{o}C and held there for 30 minutes to simulate the processing thermal conditions of CF manufacturing. The dyes were finally heated to 450 ^{o}C to determine their degradation temperature. All heating was carried out at the rate of 10 ^{o}C/min under nitrogen atmosphere [16].

2.2.6.2 Thermal stability of color filters

Prepared pigment-based and dye-based CFs were heated at 250 ^{o}C and kept for 1 hour using Jeiotech Co., Ltd. Forced Convection Oven OF-02GW. The chromaticity difference (ΔE_{ab}) values before and after heating was examined by color spectrophotometer (LCF A2000).

2.3 Results and Discussion

2.3.1 Synthesis of dyes

Prepared dyes have the same structures of corresponding thermally stable perylene and phthalocyanine pigments [17,18], but they have sulfonic acid groups. Sulfonation of 3,4,9,10-perylenebis(dicarboximide) derivatives (**2a-d**) in oleum gave disulfonate derivatives of 3,4,9,10-perylenebis(dicarboximide). Sulfonation in air gave a mixture of isomeric 1,7-disulfo-3,4,9,10-perylenebis(dicarboximide) and 1,6- disulfo-3,4,9,10-perylenebis(dicarboximide). The proton peaks of 6-position and 7-position of perylene appeared at the same field (7.90 ~ 7.95 ppm for **2a-d**) and these were confirmed by ^{1}H-NMR. On the other hand, the sulfonation with oleum in an inert atmosphere led to the homogeneous 1,7-disulfo-3,4,9,10-perylenebis(dicarboximide).

The sulfonic acids of metal phthalocyanines were readily accessible by direct sulfonation with oleum. However, by varying the oleum concentration, reaction temperature, and time, up to four sulfonate groups could be introduced in the 4-position of the benzene ring [19,20]. The resulting products were mixtures of different regio-isomers which have slightly different polarity and solubility. Therefore, in order to obtain the homogeneous tetra-sulfonated metal phthalocyanines, the oleum concentration and reaction condition were controlled closely. In case of Co, Cu and Ni-phthalocyanine (**3a-c**), we used 20 % of oleum and the sulfonation reaction was carried out at 145 ^{o}C for 3 hours. Similarly, the tetra sufonated Zn-phthalocyaine (**3d**) was synthesized with 20 % oleum at 90 ^{o}C for 6 hours. The purity of metal-phthalocyanien dyes (**3a-d**) were identified in Matrix Assisted Laser Desorption/Ionization Time Of Flight (MALDI-TOF) mass spectrum.

2.3.2 Preparation of ink-jet printed color filter

Figure 2.1 briefly describes the direct ink-jet printing process on black matrix-patterned glass using the synthesized dyes. Compared to the presently commercialized complicated pigment dispersion process, the color stripe can be formed by ink-jet printing of color inks in one simple step. In addition, as this process does not involve photo-lithography, it saves on materials and minimizes the use of toxic solvent such as N-methylpyrrolidone.

Figure 2.2-(a) shows the image of red ink prepared with **2a** dye jetting from the ink-jet printer nozzle and the black matrix patterned glass. Figure 2.2-(b) shows the evenly patterned RGB pixel (27.0 μm × 88.0 μm × 1.2 μm) on a glass where RGB ink with the prepared dyes were successively jetted on.

However, the coating thickness of ink-jetted colorant layer was restricted to less than 1.2 μm which was the height of black matrix. For this reason, the prepared ink-jetted CF had a thickness of 0.8 μm as shown in Table 2.1.

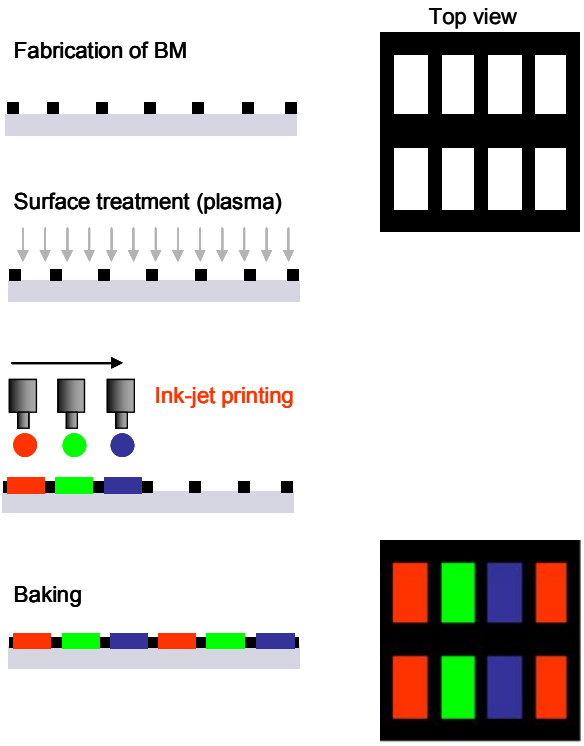

Figure 2.1 Schematic representation of ink-jet printing technology for fabrication of color filter.

(a)

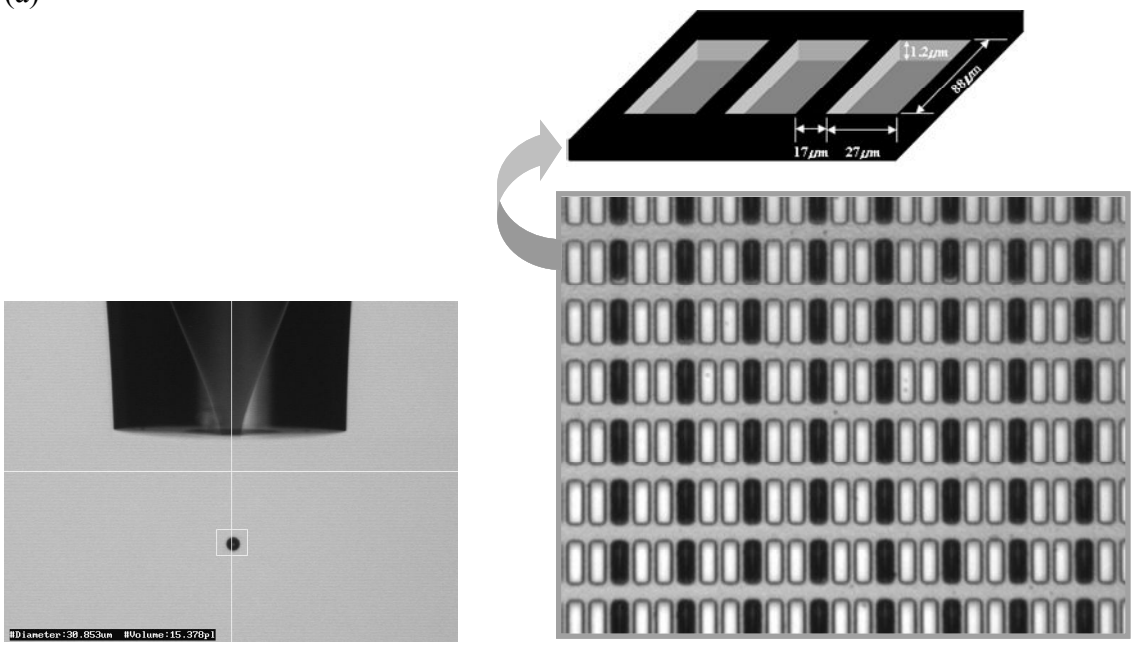

(b)

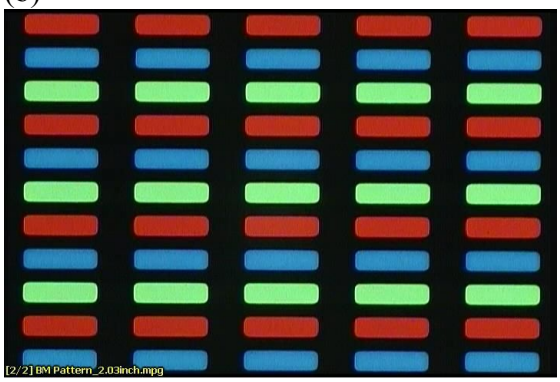

Figure 2.2 Optical microscopy (OM) image of ink-jetted sub-pixels. (a) Red ink of **2a** and **Y1** being jetted in black matrix patterned glass and gray-scale OM image of printed red stripe. (b) RGB patterned color filter using ink-jet printing method.

Table 2.1 Thermal stability of dye-based and pigment-based color filters.

	Red (ΔE_{ab})	Green (ΔE_{ab})	Blue (ΔE_{ab})	Thickness (T) (μm)
D-CF [a]	0.15	0.2	0.14	1.5
D-CF [b]	0.21	0.36	0.19	1.5
Ink-jetted D-CF [b]	0.27	0.4	0.21	0.8
P-CF	0.2	0.7	1.9	1.5

[a] Dye based color filter without color compensating dyes

[b] Dye based color filter with prepared and color compensating dyes

2.3.3 Spectral properties of dyes and dye-based color filters

Table 2.2 shows UV-Visible absorption spectra of prepared dyes in water. Dyes **2a-d** exhibited two characteristic absorption bands between 500-550 nm. The absorption maxima (λ_{max}) of dyes **2a-d** were not quite dependent upon the substituent, R. As for color strength, **2a** showed the highest molar extinction coefficient (ε_{max}) value among the dyes.

The absorption spectra of metal phthalocyanine dyes **3a-d** in water showed an intense absorption band in the range of 650-670 nm depending on the nature of the central metal atom. In these dyes, **3b** had superior absorption properties at 668 nm such as high ε_{max} value and sharp absorption band. On the other hand, **3d** showed two absorption maxima of 634 and 658 nm and it also had some absorption over 700-750 nm to make it more suitable for green colorant.

Table 2.2 UV-Visible absorption spectra of the prepared dyes in water.

Dye	λ_{max} (nm)	ε_{max} ($L \cdot mol^{-1} \cdot cm^{-1}$)	Hue
2a	500, 542	33700, 17500	Red
2b	504, 538	24100, 20600	Red
2c	502, 530	27500, 23700	Red
2d	500, 536	24600, 31100	Red
3a	658	39000	Blue
3b	668	98700	Greenish blue
3c	658	83000	Blue
3d	634, 658	67400, 68700	Bluish green

Based on spectral properties including λ_{max} and ε_{max} values of the prepared dyes, dyes **2a** (Red), **3d** (Green) and **3b** (Blue) have been chosen as colorants for LCD CF. However, these selected dyes themselves did not have accurate RGB transmittance spectra. Figure 2.3 shows the transmittance spectra of RGB CFs. For red CF, **2a** showed undesirable transmittance at 400-450 nm even though it had considerable transmittance at over 600 nm. Thus, by adding small amount of C.I. Solvent Yellow 146 (Y1) which could cut down transmittance at 400-450 nm, excellent red spectrum could be obtained. Similarly, we compensated green transmittance spectrum using C.I. Acid Yellow 1 (Y2) which decreased unnecessary transmittance at 400-450 nm. Also, we corrected blue transmittance spectrum by adding C.I. Acid Violet 43 (V1) which effectively cut down transmittance at 500-600 nm. However, transmittance at around 450 nm decreased a little bit due to the absorption of V1 at that region. Although the transmittance of the prepared CF has been somewhat lowered by color compensation, the transmittance of D-CF was higher than that of P-CF. The transmittance of red, green and blue D-CF was 92.4 %, 82.1 % and 82.9 % at 650 nm, 550 nm and 450 nm, respectively.

(a)

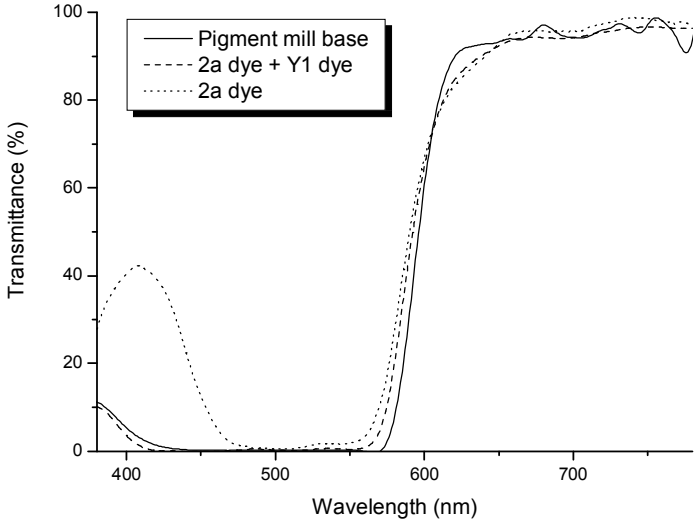

(b)

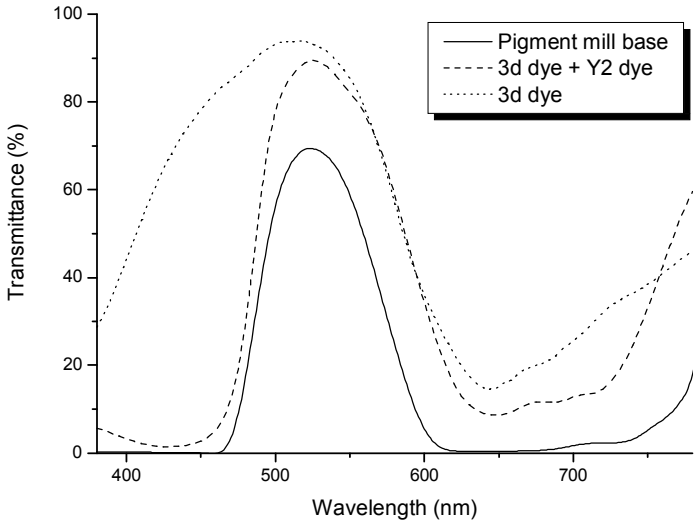

(c)

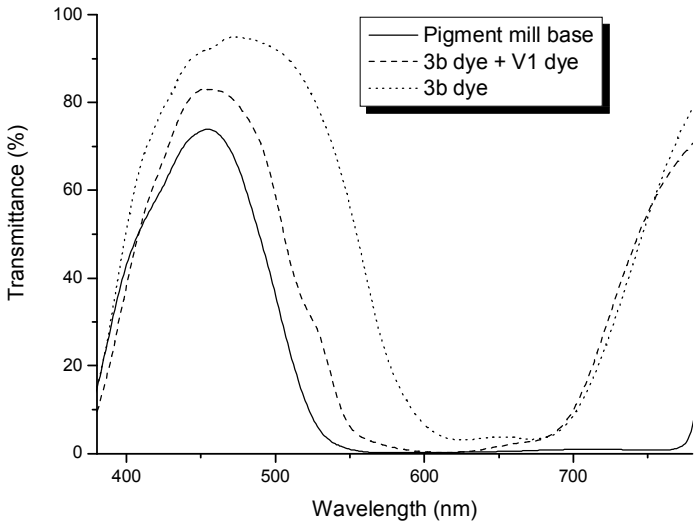

Figure 2.3 Transmittance spectra of spin-coated RGB color filters with pigments (solid line), prepare dyes (dotted line), and prepared dyes and color compensating dyes (dashed line). (a) Red color filter, (b) Green color filter and (c) Blue color filter.

Figure 2.4 and Table 2.3 compare chromaticity diagrams and coordinate values of NTSC, P-CF and D-CF. D-CF had a slightly wider color gamut than P-CF, which would improve color impression of display. D-CF also had higher brightness (Y) values than P-CF. It is known that the scattering power of the pigment particles depends upon particle size and the maximum opacity of the P-CF occurs when the diameter of particles is about half the wavelength of light, that is, about 200 nm. Thus, the smaller particle size of dyes (10 nm) than that of pigments (100 nm) lowers the scattering of incident light as shown in Figure 2.5 [21]. These enhanced transmittance and brightness can increase the contrast ratio, and consequently, a high-definition LCD will be obtained [22].

However, the chromatic property of ink-jet printed D-CF was lower than that of spin-coated D-CF. This would be due to the lower color saturation resulting from the thinner thickness (0.8 μm) of ink-jetted CF than that of spin-coated D-CF (1.5 μm). If the dye-based inks can be printed on higher black matrix (>1.5 μm) patterned glass, the chromaticity for ink-jetted D-CF would be enhanced.

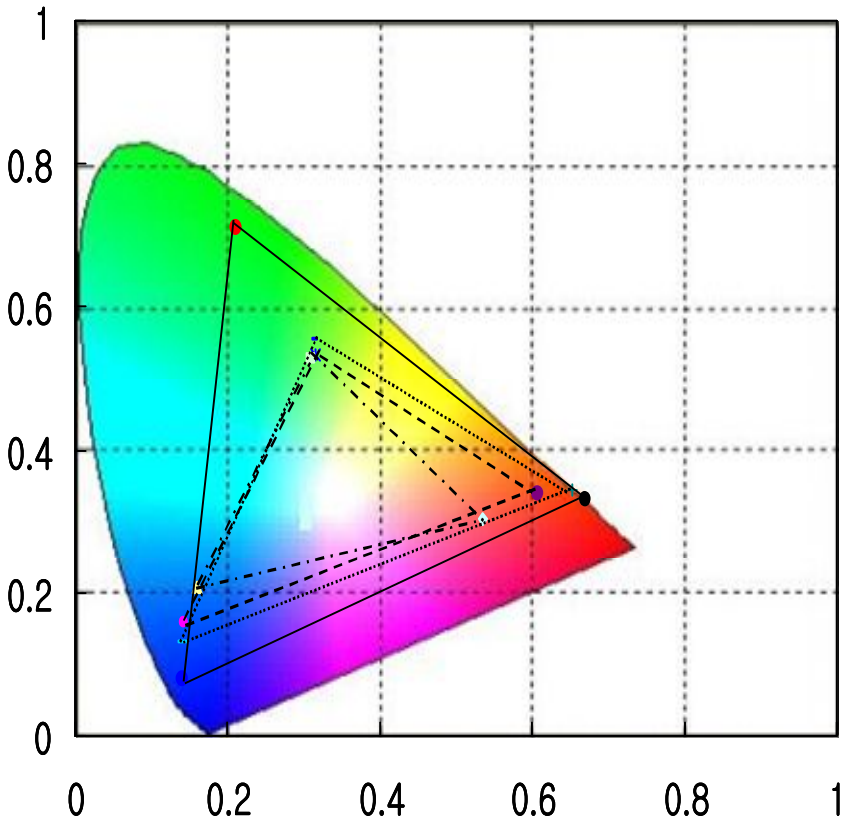

Figure 2.4 CIE 1931 chromaticity diagram of NTSC (solid line), pigment-based color filter (dashed line), dye-based color filter using spin-coating (dotted line) and dye-based color filter using ink-jet printing (dash-dotted line).

Table 2.3 The coordinate values corresponding to CIE 1931 chromaticity diagram of NTSC, pigment-based and dye-based color filter.

	Color	x	y	Y	Gamut (%)
NTSC	Red	0.670	0.330	29.0	100
	Green	0.210	0.710	60.4	
	Blue	0.140	0.080	10.4	
P-CF	Red	0.608	0.339	19.3	45.5
	Green	0.315	0.533	56.3	
	Blue	0.142	0.158	11.7	
D-CF [a]	Red	0.653	0.344	19.63	57.3
	Green	0.312	0.556	63.12	
	Blue	0.141	0.131	16.15	
D-CF [b]	Red	0.535	0.302	25.38	33.6
	Green	0.309	0.528	51.85	
	Blue	0.159	0.207	30.19	

[a] D-CF using spin-coating method (T = 1.5 μm)

[b] D-CF using ink-jet printing method (T = 0.8 μm)

(a)

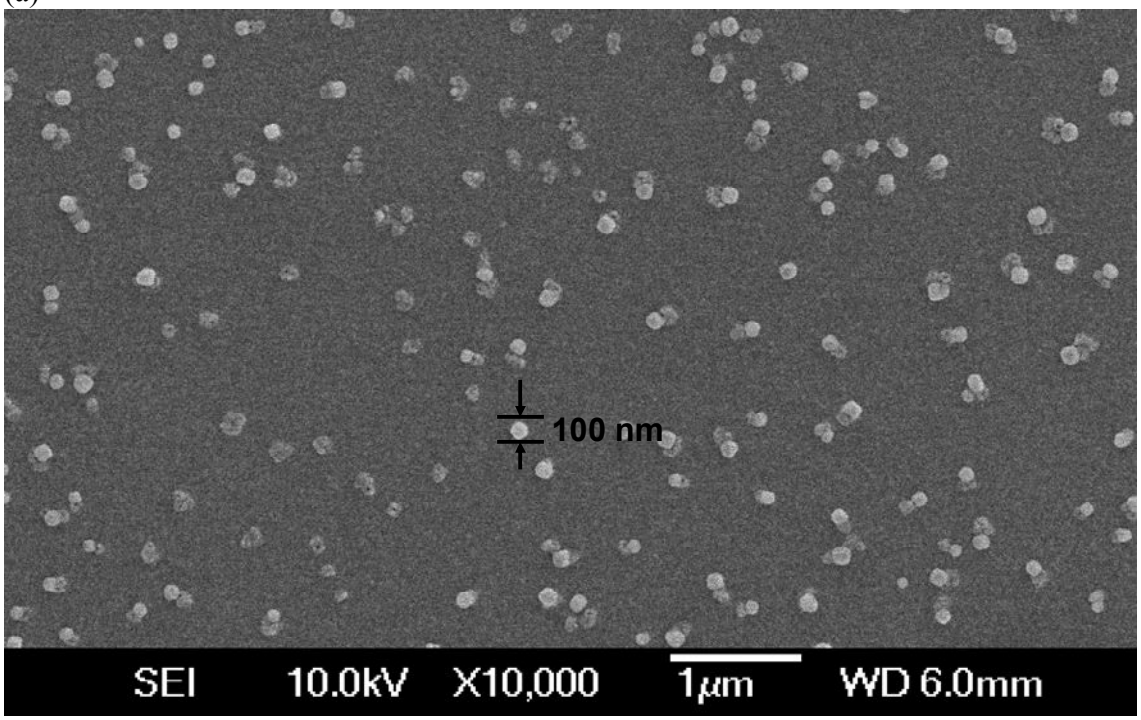

(b)

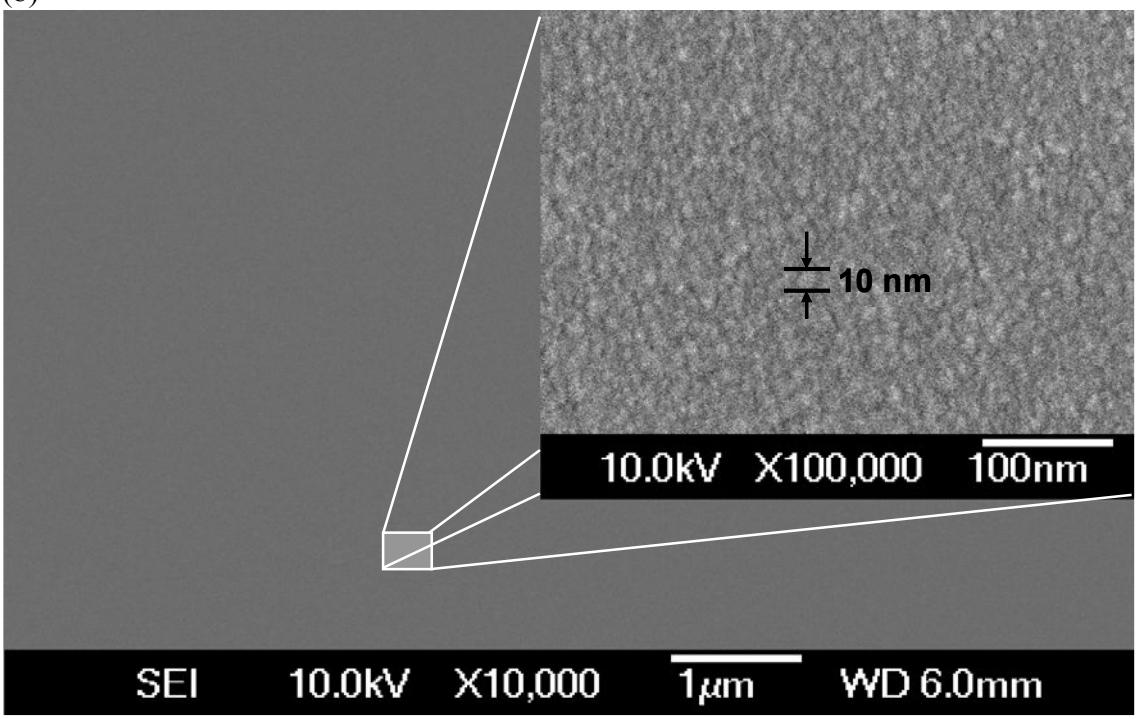

Figure 2.5 FE-SEM images of color filters. (a) pigment-based color filter with pigment-crystalline particles. (b) dye-based color filter with dye aggregates.

2.3.4 Thermal stability of dyes and dye-based color filters

In general, a material with strong intermolecular interaction has high thermal stability. For the high thermal stability, the dye molecules should have strong intermolecular interaction and form compact aggregates [23-25]. The synthesized perylene (**2a-d**) and phthalocyanine (**3a-d**) dyes have planar and symmetric molecular structure, which results in effective molecular packing through π-π interaction. In addition, their high molecular weight and polar substituent will make intermolecular interaction such as Van der Waals' Force and dipole-dipole interaction strengthened. As a result, all of the prepared dyes showed satisfactory thermal stability for manufacturing of LCD color filter.

Thermal stability of the dyes is investigated through measuring of their change in weight at 220 ^{o}C - the highest temperature in LCD manufacturing process [26,27]. Figure 2.6 shows the thermogravimetric analysis graph of synthesized dyes. The majority of dyes showed below 5 % weight loss for 30 minute maintenance at the temperature of 220 ^{o}C and they were stable up to 250 ^{o}C. Dyes **2a**, **2b** and **3b** exhibited below 1 % weight loss.

For commercial applications, CFs should have the chromaticity difference (ΔE_{ab}) values less than three after heating for an hour at 250 ^{o}C from the view point of thermal stability [24,25]. As shown in Table 2.1, the ΔE_{ab} values of D-CF both with and without color compensating dyes were similar to that of P-CF or even lower in some cases. ΔE_{ab} values of D-CF using color compensating dyes were higher than D-CF without them, which implied that the thermal stability of compensating dyes might be lower than that of the synthesized dyes. The ΔE_{ab} values of ink-jetted CFs using dyes were slightly higher than those of spin-coated CFs due to their thinner coating thicknesses. Nevertheless, the ΔE_{ab} values of ink-jetted CFs were generally lower than that of P-CF. Therefore, it can be concluded that the thermal stability of D-CFs with thermally stable dyes were not largely affected by the

manufacturing method, and the prepared dyes could be successfully applied to ink-jet printing technology.

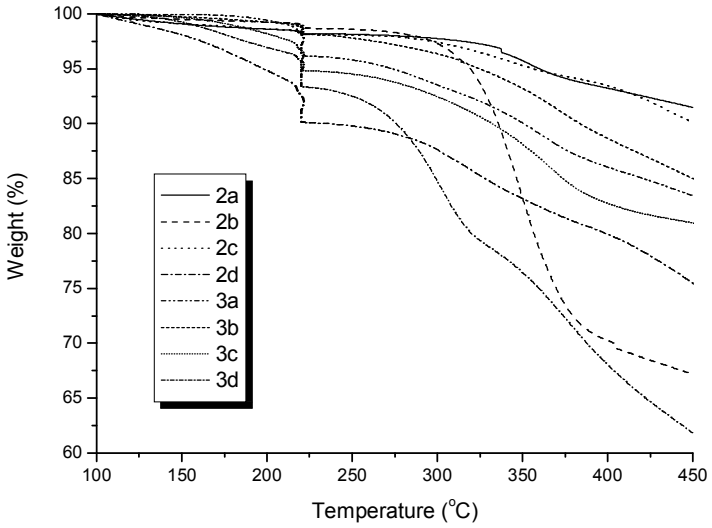

Figure 2.6 Thermogravimetric analysis (TGA) of prepared dyes.

2.4 Conclusions

Eight thermally stable RGB dyes were synthesized and LCD CFs were fabricated using some of these dyes. Adequate RGB transmittance spectra for CF could be obtained by the addition of yellow and violet color compensating dyes. Since the particle size of dyes is smaller than that of pigments, the prepared D-CF had higher optical performance than the P-CF while it showed a similar thermal resistance to the P-CF. In addition, the synthesized dyes were successfully applied to the ink-jet printing system which would be the new manufacturing technology for LCD CF. Fabricated ink-jet printed CF did not differ significantly from P-CF in terms of its thermal stability.

2.5 References

[1] Sabnis RW. Color filter technology for liquid crystal displays. Displays 1999;20;119–129.

[2] Tsuda K. Color filters for LCDs. Displays 1993;14;115–124.

[3] Takanori K, Yuki N, Yuko N, Hidemasa Y, KANG WB, Pawlowski PG. Polymer optimization of pigmented photoresists for color filter production. Jpn. J. Appl. Phys. 1998;37;1010–1016.

[4] Chigrinov VG. Liquid crystal devices: physics and applications. London: Artech House; 1999 p. 269–274.

[5] Na DY, Jung IB, Nam SY, Yoo CW, Choi YJ. The rheological behavior and dispersion properties of millbase for LCD colorfilters. Journal of the Korean Institute of Electrical and Electronic Material Engineers 2007;20;450–455.

[6] Calvert P. Inkjet printing for materials and devices. Chem. Mater. 2001;13;3299–3305.

[7] Chang CJ, Chang SJ, Shin KC, Pan FL. Improving mechanical properties and chemical resistance of ink-jet printer color filter by using diblock polymeric dispersants. Journal of Polymer Science: Part B: Polymer Physics 2005;43;3337–3353.

[8] Koo HS, Chen M, Pan PC, Chou LT, Wu FM, Chang SJ, Kawai T. Fabrication and chromatic characteristics of the greenish LCD colour-filter layer with nano-particle ink using inkjet printing technique. Displays 2006;27;124–129.

[9] Koo HS, Chen M, Pan PC. LCD-based color filter films fabricated by pigment-based colorant photo resist inks and printing technology. Thin Solid Films 2006;515;896–901.

[10] Hu Z, Xue M, Zhang Q, Sheng Q, Liu Y. Nanocolorants: a novel class of colorants, the preparation and performance characterization. Dyes and Pigments 2008;76;173–178.

[11] Sugiura T. Dyed color filters for liquid-crystal displays. Journal of the SID 1993;1;pp. 177–180.

[12] Yeh P, Gu C. Optics of liquid crystal displays. New York: John Wiley & Sons, Inc.; 1999 p. 270–272.

[13] Yang DK, Wu ST. Fundamentals of liquid crystal devices. New Jersey: Wiley-SID; 2006 p. 278–281.

[14] Lee KH, Ryu SM, Jung YK. Benzophenone compound and ink composition including the same. US 7164036 B2.

[15] Lee KH, Ryu SM, Jung YK. Lightfast additive having UV-absorbing moiety and ink composition including the same. US 7125442 B2.

[16] Guerrero DJ, DiMenna B, Flaim T, Mercado R, Sun S. Dyed red, green, and blue photoresist for manufacture of high-resolution color filter arrays for image sensors. Proceedings of SPIE/IS&T 2003;5017;298–306.

[17] Semyannikov PP, Basova TV, Grankin VM, Igumenov IK. Vapour pressure of some

phthalocyanines. J. Porphyrins Phthalocyanines 2000;4;271–277.

[18] Pasaogullari N, Icil H, Demuth M. Synthesis and unsymmetrical perylene diimides: Their synthesis, photophysical and electrochemical properties. Dyes and Pigments 2006;69;118–127.

[19] Linstead RP, Weiss FT. Phthalosyanines and related compounds. Part ⅩⅩ. further investigations on tetrabenzporphin and allied substances. J. Chem. Soc. 1950;2975–2981.

[20] Ali H, Langlois R, Wagner JR, Brasseur N, Paquette B, Lier JEV. Biological activities of phthalocyanines–Ⅹ. syntheses and analyses of sulfonated phthalocyanines. Photochemistry and Photobiology 1988;47;713–717.

[21] Tilley RJD. Colour and optical properties of Materials Chichester: John Wiley & Sons, Inc.; 2000 p. 108–110.

[22] Yeh P, Gu C. Optics of liquid crystal displays. New York: John Wiley & Sons, Inc.; 1999 p. 198–222.

[23] Giles CH, Duff DG, Sinclair RS. The relationship between dye structure and fastness properties. Rev. Prog. Coloration 1982;12;58–65.

[24] Das S, Basu R, Minch M, Nandy P. Heat-induced structural changes in merocyanine dyes: X-ray and thermal studies. Dyes and Pigments 1995;29;191–201.

[25] Chunlong Z, Nianchun M, Liyun L. An investigation of the thermal stability of some yellow and red azo pigments. Dyes and Pigments 1993;23;13–23.

[26] Ohmi T. Manufacturing process of flat display. JSME Int. J. Ser. B (Jpn. Soc. Mech. Eng.) 2004;47;422–428.

[27] Takamatsu T, Ogawa S, Ishii M. Color filter fabrication technology for LCDs. Sharp Tech. J. (Japan) Sharp Technical Journal 1991;50;69–72.

Chapter 3

Synthesis, application and investigation of structure-thermal stability relationships of thermally stable water-soluble azo naphthalene dyes for LCD red color filters

3.1 Introduction

Dyes have been traditionally used for the coloring of textiles. However, dyes are nowadays being employed in a range of high technology areas, such as display [1-5], energy [6-8], bio [9-11] and digital printing [12-14] industries. In particular, with the progress of display and digital printing industries, the necessity of using water-soluble dyes in these industries for the environmentally friendly organic solvent-free coloring process has increased. However, the weak thermal stability of water-soluble dyes is the main disadvantage in manufacturing dye-based LCD color filters (CFs) [15,16] and thermal type ink cartridges [17-20]. Nevertheless, there have been few systematic investigations of the thermal stability of water-soluble dyes for these purposes [21,22].

In this study, a range of water-soluble azo dyes with the same molecular weight, chemical formula and substituents were designed and synthesized. With these structurally isomeric dyes, dye-based color filters (D-CFs) were fabricated by spin-coating on transparent glass substrates. The absorbance, transmittance and chromaticity of the color filters were measured by UV-Vis spectrophotometry and colorimetry. In addition, their total energies and bond lengths for intra-molecular interactions, densities and molecular packing geometries for

inter-molecular interactions were investigated to determine relationships between structure and thermal stability of the structurally isomeric dyes.

3.2 Experimental

3.2.1 Materials and instrumentation

5-Amino-1-naphthalenesulfonic acid (Laurent's acid), 5-amino-2-naphthalenesulfonic acid (1,6-Cleve's acid), 6-amino-1-naphthalenesulfonic acid (Dahl's acid), 6-amino-2-naphthalenesulfonic acid (Bronner's acid), and 2,4-dinitro-1-naphthol-7-sulfonic acid disodium salt (C.I. Acid Yellow 1) were purchased from TCI. 4-Hydroxy-2,7-naphthalenedisulfonic acid disodium salt (Rudolf Guercke acid) and 3-hydroxy-2,7-naphthalenedisulfonic acid disodium salt (R acid) were obtained from SigmaeAldrich. All the above chemicals were used as received. All other reagents and solvents used were of reagent-grade quality. Transparent glass substrates were provided by Paul Marienfeld GmbH & Co. KG. Commercial acrylic binder of KGAP-823 was supplied by APEC Co., Ltd.

The ^{1}H nuclear magnetic resonance (NMR) spectra were recorded on a Bruker Avance 500 spectrometer at 500 MHz using DMSO-d_6 and TMS, as the solvent and internal standard, respectively. The mass spectra were recorded in fast atom bombardment (FAB) ionization mode using a JEOL JMS-AX505WA/HP 6890 Series II Gas Chromatography-Mass Spectrometer. The absorption and transmittance spectra were measured on a HP8452A spectrophotometer. Density data of the dyes was collected from a Micromeritics AccuPyc 1330 density analyzer. Thermogravimetric analysis (TGA, Thermogravimetric Analyzer 2050, TA Instruments) and Differential Scanning Calorimetry (DSC, Differential Scanning

Calorimeter 2920, TA Instruments) were carried out under nitrogen at a heating rate of 10 K/min. Intra- and intermolecular interactions of the dye molecules were calculated by Dmol^3 and Discover embedded in a Materials Studio 4.3 (Accelrys, USA). The chromatic characteristics of the color filters were analyzed using an Otsuka Electronics LCF A2000 spectrometer. The thickness of the color filters was measured using a Nano System Nanoview E-1000.

3.2.2 Synthesis of dyes

Figures 3.1 and 3.2 show the synthetic scheme of the dyes and their structures, respectively. All dyes were synthesized as previously described through direct diazotization [23,24] of 5-amino-1-naphthalenesulfonic acid (**1**), 5-amino-2-naphthalenesulfonic acid (**2**), 6-amino-1-naphthalenesulfonic acid (**3**) and 6-amino-2-naphthalenesulfonic acid (**4**), followed by the coupling of the diazonium salts with 4-hydroxy-2,7-naphthalenedisulfonic acid disodium salt (**a**) and 3-hydroxy-2,7-naphthalenedisulfonic acid disodium salt (**b**) in an alkaline medium [25]. After adding sodium chloride to the solution, the precipitate formed was filtered, washed with ethanol and dried in a vacuum oven at 40 ^{o}C. The crude product was heated in ethanol for 2 h under reflux, hot filtered, washed with hot ethanol and then dried in a vacuum oven. To remove the remaining sodium chloride, 2 g of the product was dissolved in 80 ml of N,N-dimethylmethanamide. The mixture solution was then poured into 600 ml of diethyl ether, and the precipitate was filtered and dried at 40 ^{o}C under vacuum. The purity of the prepared dyes was confirmed by thin layer chromatography using isopropyl alcohol/acetone/ammonia (1:2:1) as the mobile phase. Table 1 lists the yield, absorption maxima (lmax), molar extinction coefficients (3max), ^{1}H NMR and mass data of the synthesized dyes.

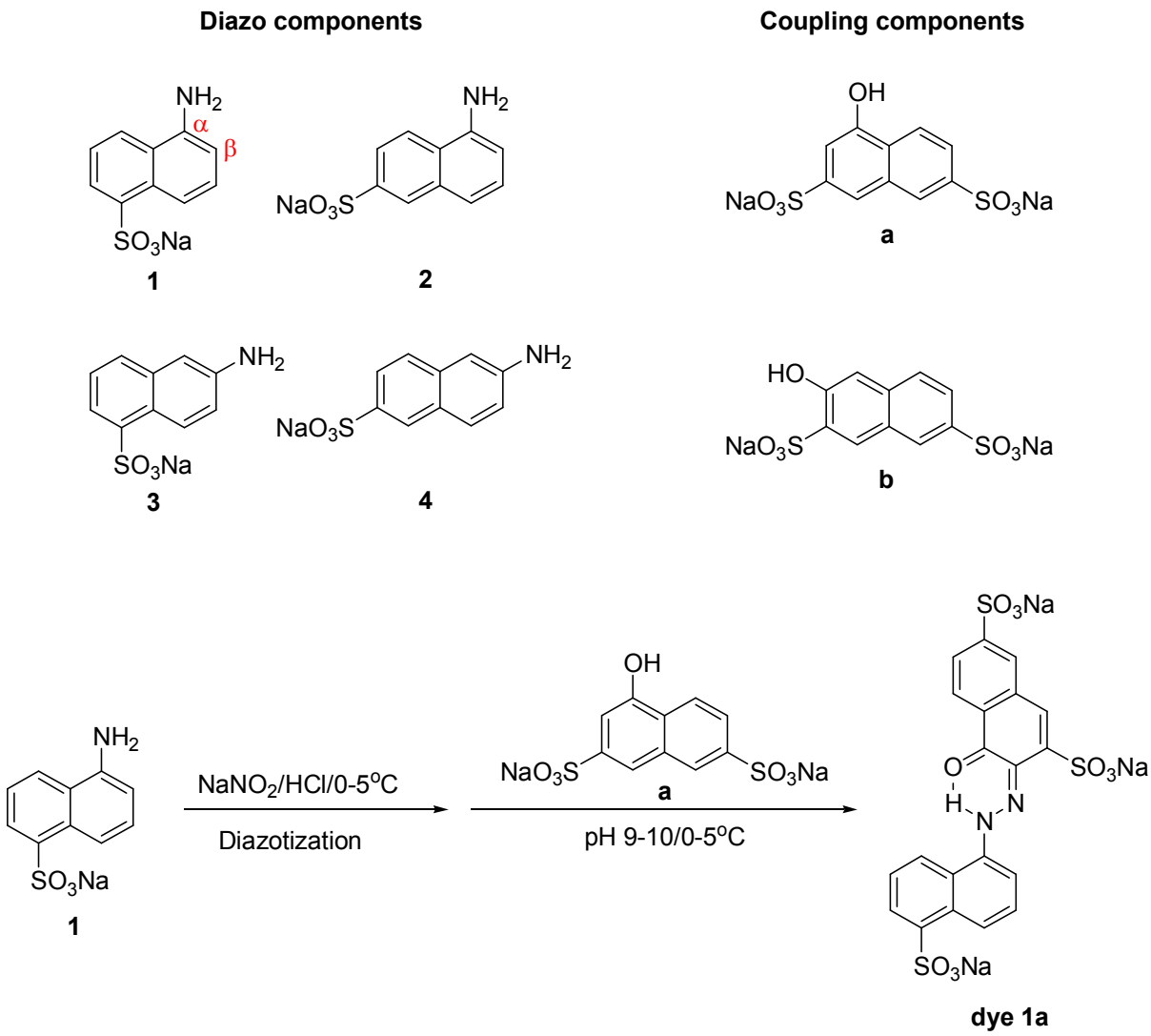

Figure 3.1 Reagents and representative synthetic scheme for the dyes studied.

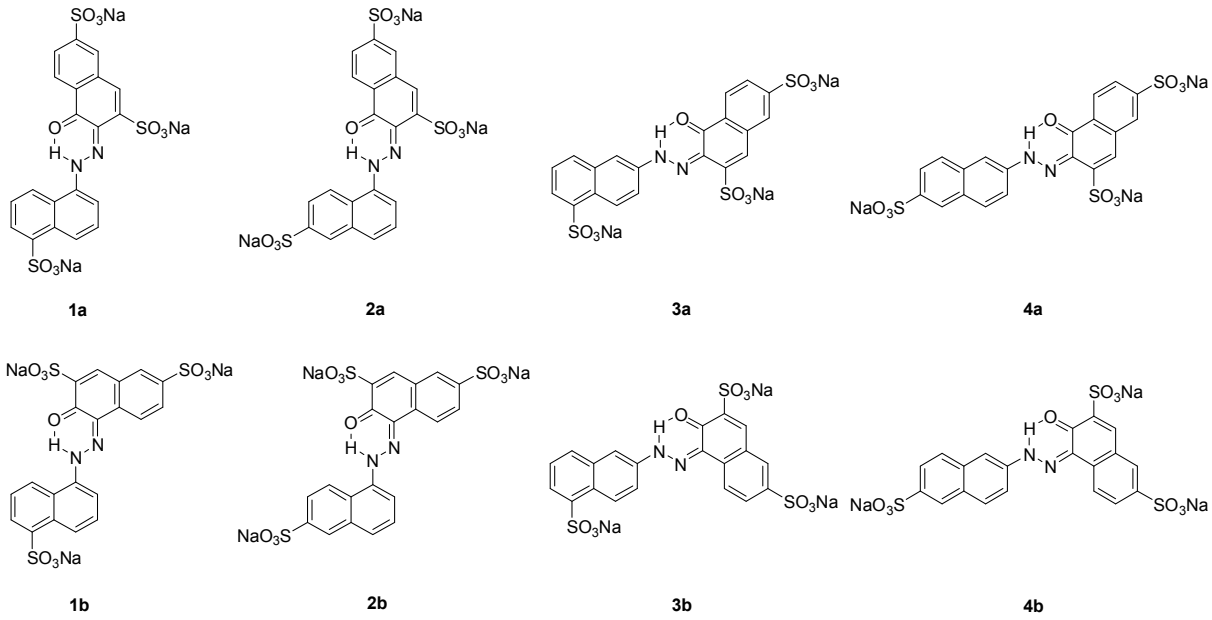

Figure 3.2 Structures of the prepared dyes.

Table 3.1. Yields, spectral properties, ^{1}H NMR and mass data of the prepared dyes

Dye	Yield (%)	λ_{max} [a] (nm)	ε_{max} [a] ($1 \cdot mol^{-1} \cdot cm^{-1}$)	^{1}H NMR (ppm, DMSO-d_6)	mass (*m/z*)
1a	68	518	21,000	7.64 (s, 1H), 7.70 (t, 1H), 7.74 (t, 1H), 7.77 (d, 1H), 7.79 (s, 1H), 8.10 (d, 1H), 8.24 (d, 2H), 8.37 (d, 1H), 8.86 (d, 1H), 17.44 (s, 1H, OH)	605 (100%, $[M+H]^+$)
1b	71	518	17,000	7.70 (t, 1H), 7.73 (t, 1H), 7.84 (s, 1H), 7.95 (s, 1H), 7.98 (d, 1H), 8.12 (d, 1H), 8.31 (d, 1H), 8.45 (d, 1H), 8.64 (d, 1H), 8.92 (d, 1H), 17.26 (s, 1H, OH)	627 (100%, $[M+Na]^+$)
2a	72	518	26,000	7.63 (s, 1H), 7.70 (t, 1H), 7.77 (d, 1H), 7.93 (s, 1H), 7.98 (d, 1H), 7.98 (d, 1H), 8.23 (d, 1H), 8.25 (d, 1H), 8.29 (s, 1H), 8.37 (d, 1H), 17.30 (s, 1H, OH)	605 (100%, $[M+H]^+$)
2b	57	518	22,000	7.73 (t, 1H), 7.84 (d, 1H), 7.95 (s, 1H), 7.96 (d, 1H), 8.01 (s, 1H), 8.03 (d, 1H), 8.29 (s, 1H), 8.33 (d, 1H), 8.39 (d, 1H), 8.60 (d, 1H), 17.30 (s, 1H, OH)	605 (100%, $[M+H]^+$)
3a	69	502	34,000	7.50 (t, 1H), 7.60 (s, 1H), 7.86 (d, 1H), 7.92 (s, 1H), 7.92 (d, 2H), 8.12 (d, 1H), 8.23 (s, 1H), 8.29 (d, 1H), 8.92 (d, 1H), 19.38 (s, 1H, OH)	627 (100%, $[M+Na]^+$)
3b	62	502	24,000	7.48 (t, 1H), 7.71 (s, 1H), 7.92 (d, 1H), 7.95 (s, 1H), 7.98 (d, 1H), 8.06 (d, 1H), 8.14 (d, 1H), 8.33 (s, 1H), 8.60 (d, 1H), 8.94 (d, 1H), 16.59 (s, 1H, OH)	627 (100%, $[M+Na]^+$)
4a	60	502	36,000	7.59 (s, 1H), 7.76 (s, 1H), 7.76 (d, 1H), 7.89 (d, 1H), 7.91 (s, 1H), 8.11 (d, 1H), 8.19 (d, 2H), 8.19 (s, 1H), 8.28 (d, 1H), 16.34 (s, 1H, OH)	605 (100%, $[M+H]^+$)
4b	63	502	26,000	7.86 (d, 1H), 7.95 (s, 1H), 8.00 (s, 1H), 8.02 (d, 1H), 8.11 (d, 1H), 8.19 (d, 1H), 8.22 (s, 1H), 8.32 (s, 1H), 8.33 (d, 1H), 8.54 (d, 1H), 16.64 (s, 1H, OH)	605 (100%, $[M+H]^+$)

[a] Measured in H_2O.

3.2.3 Preparation of dye-based inks

1 wt% of aqueous red ink was composed of the synthesized dyes (10.0 mg), distilled water (0.5 ml), and KGAP-823 (0.5 ml) as a binder based on acrylate. 5 wt% of aqueous red ink was composed of dye **4a** (30.0 mg), C.I. Acid Yellow 1 (20 mg), distilled water (0.5 ml), and KGAP-823 (0.5 ml). 10 wt% of aqueous red ink was composed of dye **4a** (60.0 mg), C.I. Acid Yellow 1 (40 mg), distilled water (0.5 ml), and KGAP-823 (0.5 ml).

3.2.4 Fabrication of dye-based color filters

The dye-based inks were coated onto a transparent glass substrate using a MIDAS SystemSPIN-1200D spin coater. The coating speed was kept for 10 s at 300 rpm. The speed was increased to 700 rpm and kept at that rate for 50 s. The wet dye-coated color filters were baked at 150 ^{o}C for 1 h. All spin coated dye-based color filters were 1.7 mm thick.

3.2.5 Quantum mechanics (QM) and molecular mechanics (MM) Calculation

To evaluate the intra-molecular interaction of the dye molecules, density functional theory (DFT) calculations were performed using the local density approximation (LDA) functional [26]. A double numerical plus d-functions (DND) was adopted as the basis set, which is embedded in the Dmo13 (Materials Studio, Accelrys,USA) [27]. The orbital cut-off distance and energy convergence were set to 4.5 A and 0.026 kJ/mol respectively. Molecular mechanics (MM) calculations were used to calculate the optimized molecular packing geometries of the prepared dyes. The DREIDING ForceField (FF) [28] was adopted to optimize the structure of dyes, which included a 6-membered ring induced by H-bonding

between –C=O and H–N–N– in the hydrazone form, because this FF is known to be moderately accurate for the optimization and calculation of the geometry, conformational energy, inter-molecular binding energy and crystal packing of organic molecules. The qEq charge equilibrium method [29], which is applicable to the sodium sulfonate ionic bond, was also used to assign the atomic charge of the dyes.

3.3 Results and discussion

3.3.1 Synthesis and spectral properties of dyes

The diazo-components of the dyes were coupled to the *ortho*-position of the hydroxyl group of the coupling components to make the dyes water-soluble. 2-Azo-1-naphthol derivatives exist mainly in hydrazone form via intra-molecular hydrogen bonds, which results in the linearity and coplanar conformation of the dyes (Figure 3.2) [30]. The proton peaks involved in intra-molecular hydrogen bonding appeared at a much lower field in the ^{1}H NMR spectrum (17.4–16.3 ppm for dyes of **1a–4b**) than the normal proton peak of the hydroxyl group [31].

Table 1 lists the spectral properties of the prepared dyes. As shown in the table, dyes coupled at the α-position of the diazo-component were bathochromic compared to those coupled at the β-position. On the other hand, the molar extinction coefficients of dyes **1a–4b** were higher than those of dyes **1a–4b**.

3.3.2 Spectral and chromatic properties of dye-based color filters

To apply a dye to LCD red color filters, the dye needs to have a sharp absorption spectrum near 500 nm and thermal stability at above 250 ^{o}C [15,16]. Figure 3.3(a) shows the absorption spectra of the fabricated color filters with 1 wt% of the prepared dyes. All the prepared red color filters had absorption maxima between 502 to 520 nm, and their molar extinction coefficients varied with the dye structure. The color filters with the **3a**, **3b**, **4a** and **4b** dyes had absorption maxima within 502 nm and 504 nm, and the color filters had high

transmittances above 600 nm, as shown in Figure 3.3(b). In particular, since dye **4a** has the highest molar extinction coefficients, the color filter using dye **4a** could have the lowest transmittance at 500 nm. However, dye **4a** had undesirable transmittance at 400-500 nm. Nevertheless, an excellent red spectrum could be obtained by adding C.I. Acid Yellow 1, which could cut down transmittance at 400-500 nm.

Figure 3.3(c) shows the transmittance spectra of the color-compensated red color filters. The red D-CF of 5 wt% and 10 wt% dye content showed 100 % and 98.9 % transmittance at 650 nm respectively. These values were 8.23 % and 7.03 % higher than 92.4 % of our previous manufactured red D-CF [15].

(a)

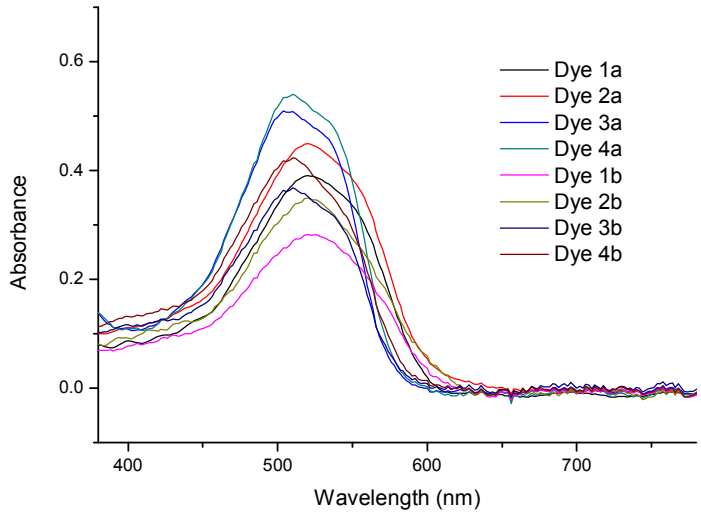
Absorbance
0.0
0.2
0.4
0.6
400
500
600
700
Wavelength (nm)
Dye 1a
Dye 2a
Dye 3a
Dye 4a
Dye 1b
Dye 2b
Dye 3b
Dye 4b

(b)

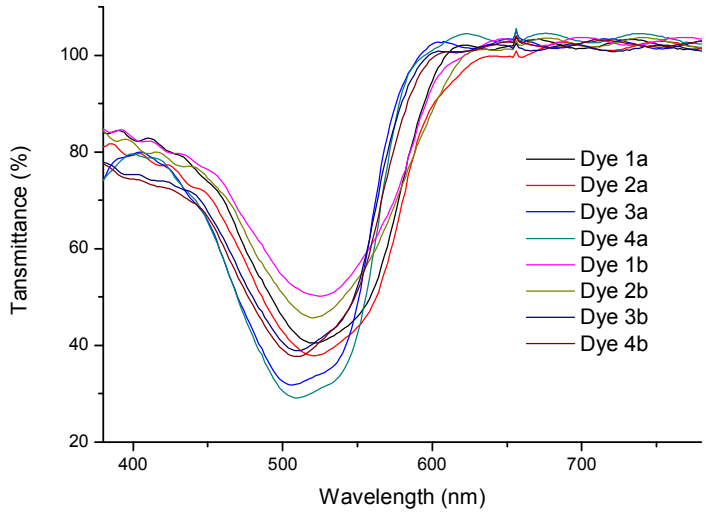
Tansmittance (%)
20
40
60
80
100
400
500
600
700
Wavelength (nm)
Dye 1a
Dye 2a
Dye 3a
Dye 4a
Dye 1b
Dye 2b
Dye 3b
Dye 4b

(c)

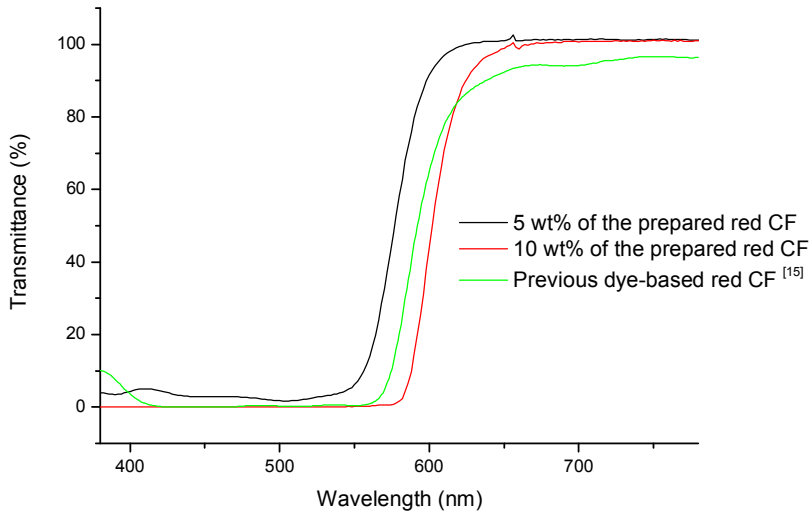

Figure 3.3 Spectral properties of the prepared color filters. (a) Absorption spectra of the fabricated color filters with 1 wt% of the prepared dyes. (b) Transmittance spectra of the fabricated color filters with 1 wt% of the prepared dyes. (c) Transmittance spectra of the color compensated red color filters with yellow dyes.

This high transmittance of the dye **4a**-based CF might be due to following three reasons. (1) The prepared water-soluble azo dyes have three sodium sulfonate water-solubilizing groups, while the water-soluble perylene dye has two sodium sulfonate groups [15]. Therefore, the azo dyes could have higher solubility in water and compatibility for the hydrophilic acrylic binder than those of the perylene dye, which resulted in the low aggregation of dye molecules in the water-based ink. Low aggregation leads to low light scattering, which could increase the transmittance of the prepared D-CFs. (2) Dye **4a** has a higher molar extinction coefficient than the perylene dye used in previous red D-CF [15]. Therefore, the red D-CF with dye **4a** could have a lower dye content, which results in higher transmittance than the previous red D-CF. (3) The C.I. Acid Yellow 1 (2,4-dinitro-1-naphthol-7-sulfonic acid disodium salt) color compensating dye can be dissolved easily in the media (water) and has higher compatibility with the water-soluble binder than the Solvent Yellow 146 (metal free mono azo dye) color compensating dye for the previous red D-CF due to its sulfonic acid group [15]. Therefore, the higher solubility in water and compatibility with the binder of Acid Yellow 1 may result in less aggregation in the water-based ink, which could enhance the transmittance of the prepared red D-CF.

In addition, as shown in Figure 3.4, the D-CF with dye **4a** and Acid Yellow 1 had wider color gamut of 62.8 % than the previous D-CF, which had a value of 57.3 %, even though the CF had lower dye content than the previous D-CF (10 wt.% vs. 15 wt%) [15]. This could be due to the high molar extinction coefficient of dye **4a**.

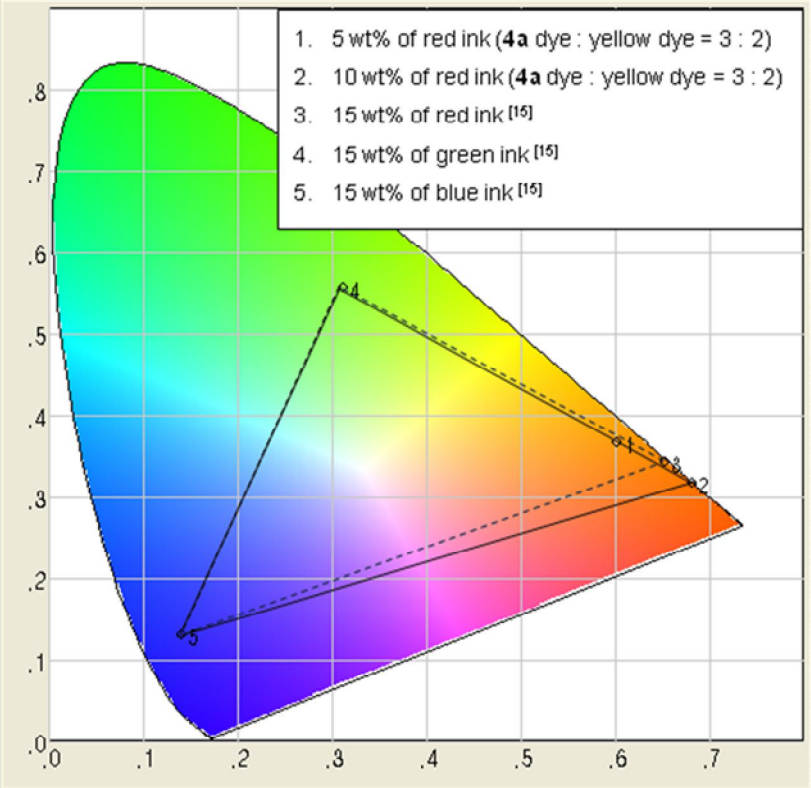

Figure 3.4 CIE 1931 chromaticity diagram of the prepared dye-based color filter (solid line) and previous dye-based color filter (dashed line).

3.3.3 Structure-thermal stability relationships of dyes

All the prepared dyes showed degradation temperatures of above 280 ^{o}C (Figure 3.5). However, the degradation temperatures varied according to the structure of the prepared dyes. This structural difference in the dyes will result in a change in the intra- and inter-molecular interactions of the dyes. Therefore, it is only logical to assume that the thermal stability of the prepared dyes is related to the intra- and inter-molecular interactions between the dye molecules. The effect of the intra and inter-molecular interactions resulting from the structural difference in the dyes on their thermal stability are discussed.

(a)

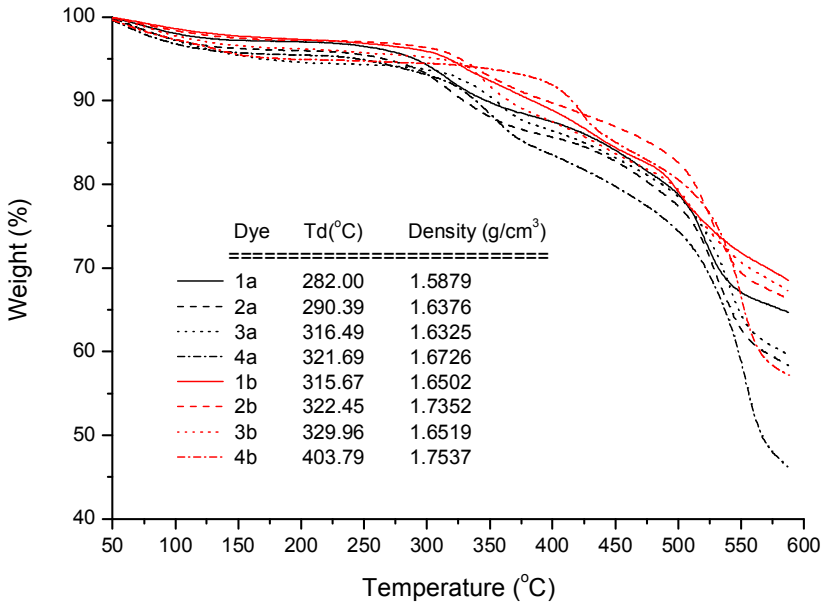

(b)

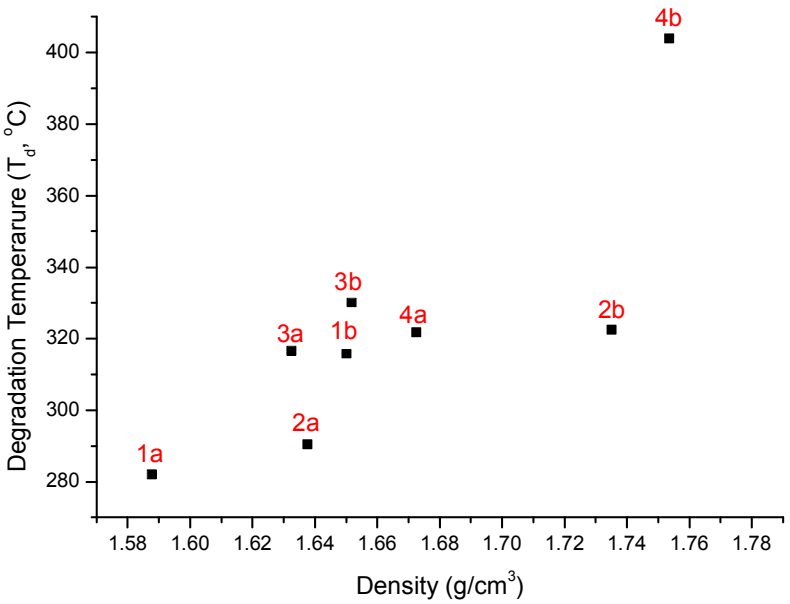

Figure 3.5 TGA and density data. (a) TGA curves, degradation temperatures and densities of the prepared dyes, (b) The relationship between degradation temperature and density. (The weight loss up to 150 °C is due to the evaporation of H_2O and DMF.)

3.3.3.1 Intra-molecular interaction of dyes

In general, hydroxyl azo dyes can cause azo-hydrazone tautomerism, and dyes with the hydrazone form and intra-molecular hydrogen bonding have higher thermal stability than those with the azo forms [30]. Therefore, when a dye shows tautomerism, the energy difference between the azo and hydrazone form could affect its thermal equilibrium. Table 3.2 shows the total energies of the prepared dyes using QM calculations. The energy differences between the hydrazone and azo forms ranged from -19.42 to -25.34 kcal/mol, as shown in the 4th column of Table 3.2. These correspond to the additional strength of the intra-molecular N-H···O hydrogen bond with a 6-membered ring structure in the hydrazone form compared to that in the azo form. Since the energy at room temperature (300 K) corresponds to 0.6 kcal/mol, most of the synthesized dyes should exist in the hydrazone forms at room temperature, which was confirmed by ^{1}H-NMR, as shown in Table 3.1.

The change in the total energies of the dye molecules can also be induced from the difference in the intra-molecular hydrogen bond length or azo bond length. The 2nd column of Table 3.3 shows that the hydrogen bond lengths of the prepared dyes were 1.516 ~ 1.535 Å, which are shorter than the general hydrogen bond length of 1.7 Å. This is due to the resonance stabilization effect of the hydrazone form with a 6-membered ring structure [32]. The 3rd and the 4th columns of Table 3.3 show the azo bond lengths of the prepared dyes. The azo form has bond lengths of 1.259 ~ 1.265 Å, whereas the bond lengths of the hydrazone are 1.288 ~ 1.293 Å. However, since the variation in hydrogen bond length and azo bond length was quite small (< 0.019 Å), it was difficult to find a meaningful relationship between the total energy and bond lengths of the dye molecules.

Table 3.2. Total energies of the prepared dyes using QM calculations.

Dye	Total energy [a]					
	Azo form	Hydrazone form	Difference of energy between azo and hydrazone form	For hydrazone form		
				Difference of **a** and **b** dyes	Dyes without $SO_3^-Na^+$	Difference of **a** and **b** dyes without $SO_3^-Na^+$
	(Ha [b])	(Ha [b])	(kcal/mol)	(kcal/mol)	(Ha [b])	(kcal/mol)
1a	- 3293.221	- 3293.259	- 24.24		- 947.1568	
				- 9.80		1.13
1b	- 3293.244	- 3293.275	- 19.42		- 947.1550	
2a	- 3293.218	- 3293.258	- 24.70		- 947.1568	
				- 10.71		1.13
2b	- 3293.243	- 3293.275	- 19.63		- 947.1550	
3a	- 3293.220	- 3293.260	- 25.34		- 947.1572	
				- 11.84		0.92
3b	- 3293.245	- 3293.279	- 21.28		- 947.1558	
4a	- 3293.224	- 3293.261	- 23.17		- 947.1572	
				- 9.66		0.92
4b	- 3293.241	- 3293.277	- 22.51		- 947.1558	

[a] energy of the geometrically optimized dye structure using DFT calculations.

[b] 1 Ha (hartree) = 627.15 kcal/mol.

Table 3.3. Bond lengths of the prepared dyes geometrically optimized with QM calculation.

Dye	Bond length (Å)				
	Hydrogen bonding of O(II) [b]···H	Azo bonding		Ionic bonding	
		Azo form (-N=N-)	Hydrazone form (-N-N=)	O(I)[a]···Na(I)[c]	O(I)[a]···Na(I)[c], O(II)[b]···Na(II)[d]
1a	1.517	1.259	1.288	2.184	-
1b	1.531	1.264	1.291	2.189	2.235, 2.241
2a	1.517	1.262	1.288	2.183	-
2b	1.529	1.263	1.291	2.190	2.232, 2.255
3a	1.517	1.259	1.288	2.182	-
3b	1.527	1.264	1.289	2.190	2.278, 2.239
4a	1.516	1.260	1.288	2.184	-
4b	1.535	1.265	1.293	2.190	2.228, 2.251

[a] O(I) is the oxygen of the sodium sulfonate salt.

[b] O(II) is the oxygen of the carbonyl groups in hydrazone formed azo dyes.

[c] Na(I) is the sodium of the general sodium sulfonate salt.

[d] Na(II) is the sodium of the specific sodium sulfonate salt, which is located at the *ortho*-position to the carbonyl group in the hydrazone formed azo dyes.

The 5th column of Table 3.2 shows the differences in the total energies of the **a** and **b** dyes. When the dyes in the hydrazone form with the same diazo-compound were compared, the total energies of dyes **1b-4b** were 9.66 ~ 11.84 kcal/mol lower than those of dyes **1a-4a**. According to QM calculations, two of the three oxygen atoms in SO_3^- interacted with Na^+ as shown in Figure 3.6. On the other hand, dyes **1b-4b** had one SO_3^- Na^+ ionic pair at the *ortho*-position of the carbonyl group. Consequently, its specific sodium cation ($Na(II)^+$) could make a multi-ionic interaction with the oxygen atom (O(II)) of the nearby carbonyl group as well as those in SO_3^-. This multi-ionic interactions of the sodium cation could strengthen the intra-molecular electrostatic attraction of dyes **1b-4b**, which results in dyes **1b-4b** having a lower total energy than dyes **1a-4a**. However, in dyes **1b-4b** as shown in Figure 3.3, with the additional Na(II)···O(II)=C attraction, the C=O(II)···H-N hydrogen bonds were 0.01~0.02 Å longer than those of dyes **1-4a** (the 2nd column of Table 3.3). Hence, the multi-ionic interaction of the sodium cation stabilized the total energy of the dye molecule, even though it decreased the strength of the intra-molecular hydrogen bond. An examination of the total energy of the hydroxyl azo naphthalene dyes without ionic sodium sulfonate functional groups revealed all the dyes to have extremely small energy differences (~ 1 kcal/mol), as shown in the 7th column of Table 3.2 (here, dyes **1a** and **2a**, **1b** and **2b**, **3a** and **4a**, and **3b** and **4b** have identical molecular structures). Therefore, the Na(II)···O(II)=C electrostatic attraction in the dye molecules lowered the total energies of dyes **1b-4b**.

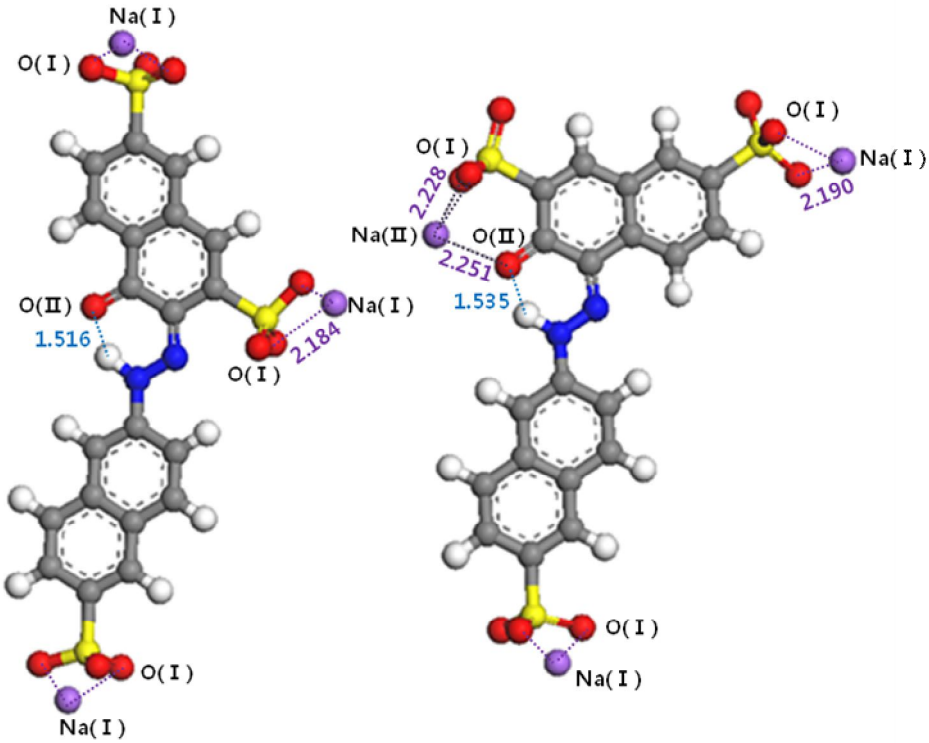

(a) (b)

Figure 3.6 The optimized molecular structure of **4a** (a) and **4b** (b) dyes by QM calculation. (unit =Å).

3.3.3.2 Inter-molecular interaction of dyes

Figure 3.5(a) shows the TGA curves and densities of the prepared dyes. The dyes decomposed at different temperatures, even though they had the same molecular weight and covalent bonding, such as C—N, C—O, C—S, N—N and N—H, etc. However, as stated in session 3.2.1, the differences in their total energies for the hydrazone form were < 12.54 kcal/mol (0.02 Ha). Judging from the above results, the change in the degradation temperatures of the dyes are believed to be related more to their inter-molecular interactions. DSC analysis was conducted to examine the inter-molecular interactions of the dyes, but their melting peaks could not be confirmed. This is different from the general melting and decomposition behavior of dyes, and the results of a study of the decomposition behavior of the prepared dyes will be reported in a separate paper.

Since a dye with a stronger inter-molecular interaction could have a higher density than the others, the inter-molecular interactions of the prepared dyes of structural isomers could be examined by comparing their densities. Fig. 5(b) shows the relationship between the degradation temperatures and densities of the prepared dyes. The degradation temperatures generally increased with increasing density. Therefore, the thermal stability of the prepared dyes was related to their density.

The density of a dye is related to its molecular packing geometry, which could be evaluated by MM calculations. Figure 3.7 shows the representative packing structure of dye **4b**. The dye molecules are aggregated three-dimensionally via strong electrostatic attractions between the three pairs of sodium sulfonate groups. Due to this aggregation behavior, all the prepared dyes had high thermal stability (T_d > 280 ^{o}C). This optimization of the molecular packing geometry can be affected by the change in electrostatic attraction, steric hindrance and linearity of dye molecules.

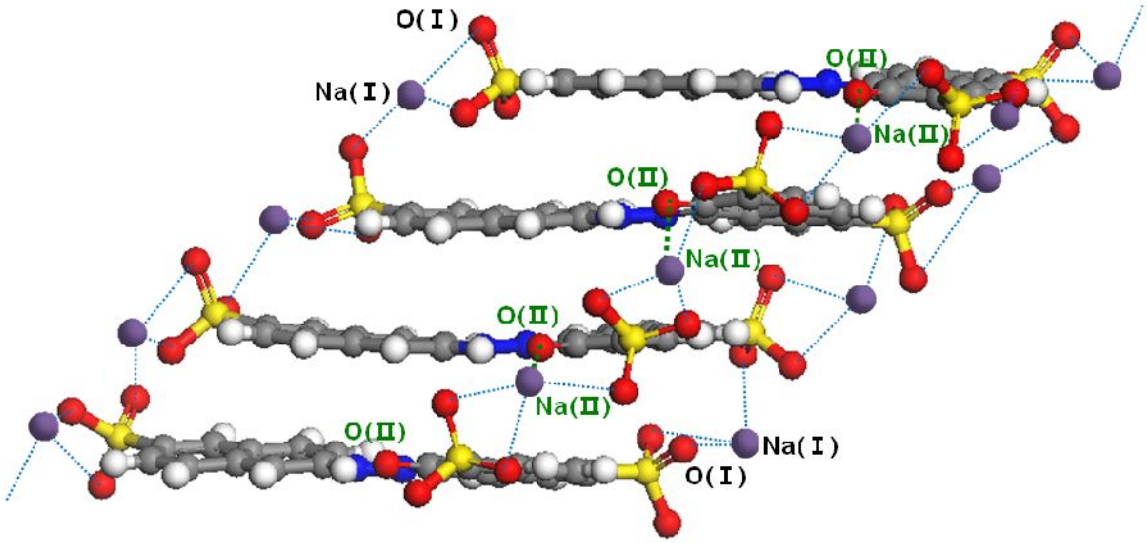

Figure 3.7 The representative packing structure of dye **4b** by MM calculation.

3.3.3.2.1 Effect of electrostatic attraction

Dyes **1b**-**4b** (red lines) generally show higher degradation temperatures and densities than those of dyes **1a**-**4a** (black lines), as shown in Figure 3.5(a). In the case of dyes **1a**-**4a**, all sodium sulfonate (SO_3^- Na^+) groups of the dyes make the general salt form by ionic interaction. However, in dyes **1b**-**4b**, there is a specific sodium sulfonate group that is located at the *ortho*-position to the carbonyl group in the hydrazone form. This can make an additional electrostatic attraction with O(II) of the adjacent carbonyl group (Figure 3.6). In addition, $Na(II)^+$ can make an multi-ionic interaction with C=O(II) and $SO(I)_3$ of the neighboring dye molecules, which can strengthen the inter-molecular electrostatic attractions as well as the intra-molecular electrostatic attractions of the dyes, as shown in Figure 3.7 and the 5th column of Table 2. Consequently, due to the more effective packing of dyes **1b**-**4b** than that of dyes **1a**-**4a**, the densities of dyes **1b**-**4b** can be increased, resulting in an increase in their degradation temperature.

3.3.3.2.2 Effect of steric hindrance

In order for the prepared dyes to have dense packing geometry, the strength of the inter-molecular electrostatic attractions between the three pairs of sodium sulfonate groups should be similar and there should be no torsion in the dye molecule. Dyes **2b** and **4b** had higher degradation temperatures than dyes **1b** and **3b**. These results might be caused by steric hindrance of the pendant sulfonate group of the diazo-component. Figure 3.8 shows the optimized packing geometries of dyes **1b**-**4b** according to MM calculations. In the case of dyes **2b** and **4b**, the adjacent dye molecules were packed parallel due to the well-balanced electrostatic attractions between the three pairs of sodium sulfonate groups. On the other hand,

in dyes **1b** and **3b**, the electron rich sodium sulfonate group in the diazo-component pushes the electron rich aromatic ring of the adjacent dye molecule and distorts the parallel molecular packing structure. Therefore, dyes **2b** and **4b** could have a more compact molecular packing structure with higher density, which would result in higher degradation temperatures than dyes **1b** and **3b**.

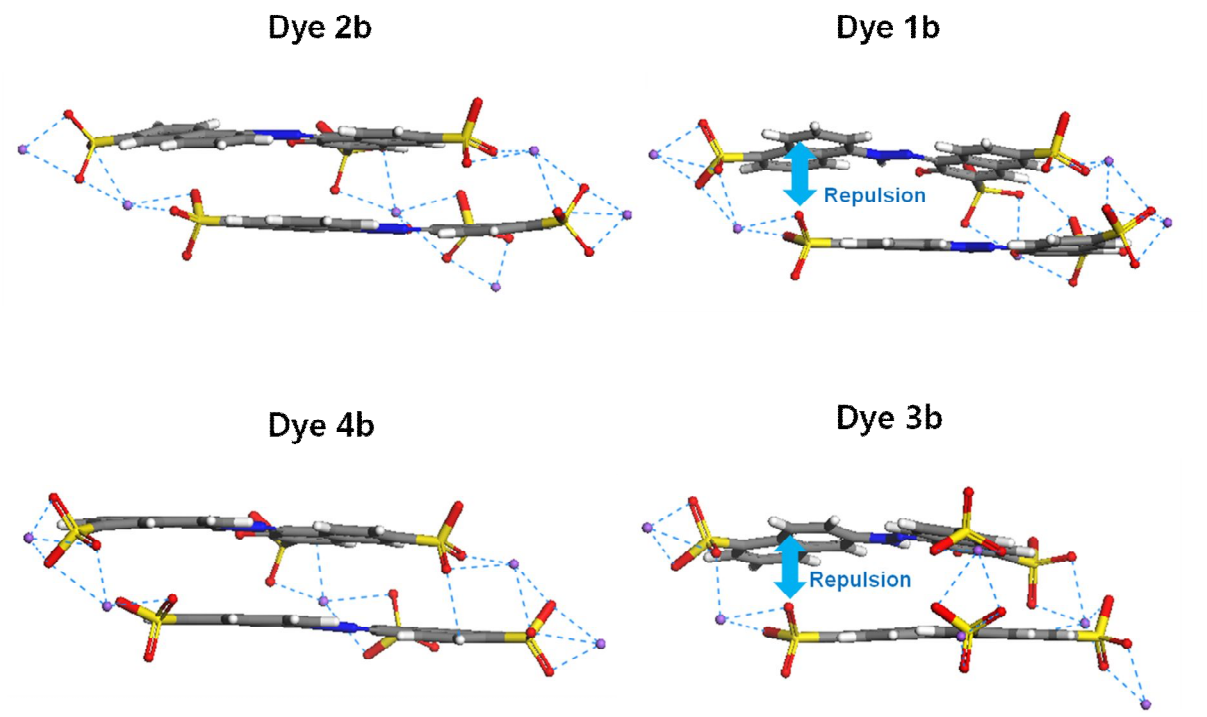

Figure 3.8 The optimized packing geometries of the dyes **1b**-**4b** by MM calculation.

3.3.3.2.3 Effect of linearity

The linearity of the dye molecules studied was affected by the position of the amine group in the diazo-component. The dye coupled at the β-position of the diazo-component had a more linear structure than the dye coupled at the α-position of the diazo-component [32,33]. The degradation temperatures of dyes **4b** and **3b** were higher than those of dyes **2b** and **1b** (Figure 3.5). As shown in Figures 3.1 and 3.2, dyes **4b** and **3b** have diazo-components with amine groups substituted at the β-position of the naphthalene ring, which results in a more linear structure. Therefore, dyes **4b** and **3b** may have denser packing structures which could increase the degradation temperature compared to dyes **2b** and **1b**.

3.4 Conclusion

Eight structurally isomeric water-soluble azo dyes were synthesized and their thermal stabilities were examined. All the prepared dyes showed high degradation temperatures (above 280 ^{o}C), while they did not have clear melting temperatures. This might be caused by the aggregation behavior by the strong inter-molecular electrostatic attractions.

Red color filters with the prepared dyes had absorption maxima between 500 nm and 520 nm. The optimal color filter was fabricated with dye **4a** and commercial yellow dye, which showed 98.9 % transmittance and a 62.8 % color gamut. Its transmittance and color gamut were improved by 7.03% and 9.6%, respectively, compared to the previous dye-based color filter.

The degradation temperatures of the prepared dyes varied according to their structure,

and the structure - thermal stability relationships were examined using the prepared structurally isomeric dyes. The prepared dyes had similar intra-molecular interactions but their thermal stability increased in proportion to their inter-molecular interactions, which could be represented by their densities. MM calculations of the molecular packing structure of the prepared dyes suggested that the electrostatic attraction, steric hindrance and linearity of the dyes could be changed by the position of the azo linkage and sodium sulfonate groups. When the dyes had multi-ionic interactions and linear structures, they could have dense molecular packing structures. On the other hand, steric hindrance between the neighboring dye molecules disturbed the effective molecular packing. The results of MM calculations of the molecular packing corresponded to those of density analysis. In conclusion, for application of the dyes in LCD color filters, dyes with more compact packing structures may have higher density values and degradation temperatures.

3.5 References

[1] Hu Z, Xue M, Zhang Q, Sheng Q, Liu Y. Nanocolorants: a novel class of colorants, the preparation and performance characterization. Dyes and Pigments 2008;76:173–178.

[2] Koo HS, Chen M, Pan PC, Chou LT, Wu FM, Chang SJ, Kawai T. Fabrication and chromatic characteristics of the greenish LCD colour-filter layer with nano-particle ink using inkjet printing technique. Displays 2006;27:124–129.

[3] Sabnis RW. Color filter technology for liquid crystal displays. Displays 1999;20:119–129.

[4] Sugiura T. Dyed color filters for liquid-crystal displays. Journal of the SID 1993;1:177–180.

[5] Tsuda K. Color filters for LCDs. Displays 1993;14:115–124.

[6] O'Regan B, Grätzel M. A low-cost, high-efficiency solar cell based on dye-sensitized colloidal TiO_2 films. Nature 1991;353:737–740.

[7] Bai Y, Cao Y, Zhang J, Wang M, Li R, Wang P, Zakeeruddin S. M, Grätzel M. High-performance dye-sensitized solar cells based on solvent-free electrolytes produced from eutectic melts. Nature materials 2008;7:626–630.

[8] Kim S, Lee JK, Kang SO, Ko J, Yum JH, Fantacci S, Angelis F, Censo D, Nazeeruddin MK, Grätzel M. Molecular engineering of organic sensitizers for solar cell applications. J. Am. Chem. Soc. 2006;128:16701–16707.

[9] Dolmans D. E., Fukumura D, Jain R. K. Photodynamic therapy for cancer. Nature Reviews Cancer 2003;3:380–387.

[10] Zhou L, Zhou JH, Dong C, Ma F, Wei SH, Shen J. Water-soluble hypocrellin a nanoparticles as a photodynamic therapy delivery system. Dyes and Pigments 2009;82:90–94.

[11] Gorman S.A, Bell A.L, Griffiths J, Roberts D, Brown S.B. The synthesis and properties of unsymmetrical 3,7-diaminophenothiazin-5-ium iodide salts: Potential photosensitisers for photodynamic therapy. Dyes and Pigments 2006;71:153–160.

[12] Calvert P. Inkjet printing for materials and devices. Chem. Mater. 2001;13:3299–3305.

[13] Yang Y, Naarani V. Improvement of the lightfastness of reactive inkjet printed cotton. Dyes and Pigments 2007;74:154–160.

[14] Hladnik A, Muck T. Characterization of pigments in coating formulations for high-end ink-jet papers. Dyes and Pigments 2002;54:253–263.

[15] Kim YD, Kim JP, Kwon OS, Cho IH. The synthesis and application of thermally stable dyes for ink-jet printed LCD color filters. Dyes and Pigments 2009;81:45–52.

[16] Chang CJ, Chang SJ, Shin KC, Pan FL. Improving mechanical properties and chemical resistance of ink-jet printer color filter by using diblock polymeric dispersants. Journal of Polymer Science: Part B: Polymer Physics 2005;43:3337−3353.

[17] Ohya H, Morimoto H. Water based ink composition and image forming method. US 2001/0023652 A1.

[18] Ishizuka T, Hokazono H, Yamanouchi J. Color composition, ink for ink-jet recording and ink-jet recording method. US 6670410 B2.

[19] Koga N, Goto K, Kobayashi N, Aoyama M, Higashiyama S, Fujioka M. Water base ink for ink-jet recording. US 6648463 B2.

[20] Oki Y, Kitamura K, Aoyama T, Uotani N, Takahashi H, Ito Y. Aqueous Ink. US 2002/0050226 A1.

[21] Lee JJ, Lee WJ, Choi JH, Kim JP. Synthesis and application of temporarily solubilised azo disperse dyes containing β-sulphatoethylsulphonyl group. Dyes and Pigments 2005;65:75–81.

[22] Koh J, Kim JD, Kim JP. Synthesis and application of a temporarily solubilised alkali-clearable azo disperse dye and analysis of its conversion and hydrolysis behavior. Dyes and Pigments 2003;56:17–26.

[23] Zollinger H. Diazo chemistry I: aromatic and heteroaromatic. New York: VCH; 1994. p. 11–20.

[24] Fierz-David H.E, Blangey L. Fundamental processes of dye chemistry. New York: Interscience; 1949. p. 241–249.

[25] Fierz-David H.E, Blangey L. Fundamental processes of dye chemistry. New York: Interscience; 1949. p. 262–269.

[26] Perdew JP, Wang Y. Accurate and Simple Analytic Representation of the Electron-Gas Correlation-Energy. Physical Review B 1992;45(23):13244–13249.

[27] Delley B. An All-Electron Numerical-Method for Solving the Local Density Functional for Polyatomic-Molecules. Journal of Chemical Physics 1990;92:508–517.

[28] Mayo SL, Olafson BD, Goddard WA. Dreiding - a Generic Force-Field for Molecular

Simulations. Journal of Physical Chemistry 1990;94(26):8897–8909.

[29] Rappe AK, Goddard WA. Charge Equilibration for Molecular-Dynamics Simulations. Journal of Physical Chemistry 1991;95(8):3358–3363.

[30] Gordon P.F, Gregory P. Organic chemistry in colour. Berlin: Springer-Verlag; 1983. p. 96–108.

[31] Skrabal P, Zollinger H. Mechanism of azo coupling reactions: part XXXV. pH-dependence and ortho/para ratio in coupling reactions of amino-hydroxynaphthalenesulfonic acids. Dyes and Pigments 1988;9:201–7.

[32] Song DH, Kim JP. Effect of transition moments and orientational behavior of dichroic dyes on the optical anisotropy of poly(vinyl alcohol) polarizing films. Dyes and Pigments 2009;80:219–225.

[33] Song DH, Yoo HY, Kim JP. Synthesis of stilbene-based azo dyes and application for dichroic materials in poly(vinyl alcohol) polarizing films. Dyes and Pigments 2007;75:727–731.

Chapter 4

A study on thermal decomposition behavior of some water-soluble azo dyes

4.1 Introduction

Azo dyes are the most versatile class of synthetic dyes since they are relatively economical to produce and have a full color spectrum with high color strength [1]. Recently, azo dyes are used in high-tech applications involving electrochromic devices [2,3], photodynamic therapy [4-7], digital printing [8-12], solar cells [13-17], and displays [18-21]. Especially with the development of display and digital printing industries, the demand for water-soluble azo dyes has been growing in regards to the environmentally friendly organic solvent-free coloring process. However, water-soluble dye-based LCD coloring materials are not widely used for the commercial manufacturing process due to the unsatisfactory thermal resistance of dyes [22-23]. Also, there is little information found pertaining to their thermal stability.

In this study, a series of structurally isomeric water-soluble dyes were synthesized. Thermal properties of the prepared dyes were examined by TGA and DSC. Their thermal decomposition process was also investigated by analyzing UV-Vis. absorbance of the prepared water-soluble dyes in various degradation temperatures. In addition, a new thermal decomposition mechanism for the prepared water-soluble hydroxyl azo dyes was suggested

via density analysis, X-ray diffraction (XRD), dynamic light scattering (DLS) and density functional theory (DFT) calculation.

4.2 Experimental

4.2.1 Materials and instrumentation

5-amino-1-naphthalenesulfonic acid (Laurent's acid), 5-amino-2-naphthalenesulfonic acid (1,6-Cleve's acid), 6-amino-1-naphthalenesulfonic acid (Dahl's acid), 6-amino-2-naphthalenesulfonic acid (Bronner's acid), 2-naphthol from TCI and 4-hydroxy-2,7-naphthalenedisulfonic acid disodium salt (Rudolf Guercke acid), 3-hydroxy-2,7-naphthalenedisulfonic acid disodium salt (R acid) and 1-naphthylamine from Sigma-Aldrich were used without further purification. All other reagents and solvents used were of reagent-grade quality.

^{1}H-NMR spectra were recorded by a Bruker Avance 500 at 500MHz using DMSO-d_6 as the solvent and TMS as the internal standard. Mass spectra were recorded in fast atom bombardment (FAB) ionization mode with a JEOL JMS-AX505WA/HP 6890 Series II Gas Chromatography-Mass Spectrometer. Absorption spectra were measured on a HP8452A spectrophotometer. Thermogravimetric analysis (TGA) and Differential Scanning Calorimeter (DSC) was conducted under nitrogen at a heating rate of 10K/min with a TA Instruments Thermogravimetric Analyzer 2050 and TA Instruments Differential Scanning Calorimeter (DSC) 2920. Small-angle X-ray scattering (SAXS) was conducted with the general area detector diffraction system (GADDS, Bruker, Germany). Particle sizes of dye

aggregates were measured by CILAS Particle Size Analyzer 1064LD.

4.2.2 Synthesis of dyes

All water-soluble hydroxyl azo dyes were synthesized by the same scheme as shown in Figure 3.1. Their structures are previously illustrated in Figure 3.2. Absorption maxima (λ_{max}), molar extinction coefficients (ε_{max}), ^{1}H NMR and Mass data of synthesized dyes are described in Chapter 3.

A water-insoluble hydroxyl azo dye was synthesized as follows to compare its degradation mechanism with water-soluble dyes [24,25]. 1-naphthylamine (1.43 g, 0.01 mol) was dissolved in 50 ml water containing concentrated hydrochloric acid (4.8 ml) at room temperature. The solution was cooled to 0-5 ^{o}C and 10 ml of sodium nitrite (0.7 g, 0.01 mol) solution was added. The diazotization was continued for 2 hrs. For coupling solution, 2-naphthol (1.44 g, 0.01 mol) was dissolved in 50 ml ethanol. The prepared diazonium salt solution was added into the coupling component solution and temperature was maintained at 0-5 ^{o}C. Sodium acetate ethanol solution (1 M) was added into the solution so as to adjust pH between 8 and 9. The mixture solution was stirred for 2 hrs, and then the dye was filtered off with suction and washed with methanol until drops of filtrate appeared colorless. The dye was then washed with hot water, dried in a vacuum oven at 40 ^{o}C. Yield 81.5 %; ^{1}H-NMR (DMSO-d_6, ppm): 9.83 (s, Ar-OH), 8.21 (d, Ar-H), 8.16 (d, Ar-H), 8.07 (d, Ar-H), 8.03 (d, Ar-H), 7.99 (d, Ar-H), 7.67 (d, Ar-H), 7.63 (d, Ar-H), 7.52 (t, Ar-H), 7.51 (t, Ar-H), 7.49 (t, Ar-H), 7.46 (t, Ar-H), 7.35 (t, Ar-H), 7.17 (d, Ar-H); GC-MS: *m/z* 298.11 (100%, M^+).

4.2.3 Measurement of the relative absorbance of the prepared dyes in various temperatures

From 250 ^{o}C to 450 ^{o}C, the prepared dyes were baked at every 50 ^{o}C and their loss of color strength was monitored. Absorbances (A_T) of the baked dyes at each temperature (T) were measured by a UV-Vis. spectrophotometer. To compare absorption intensity for each prepared dyes, the relative absorbance (A_R) of the prepared dyes were calculated by the following Eq. (1) and presented in Table 4.1.

$$A_R = A_T/A_0 \times 100 \quad \cdots\cdots\cdots\cdots \quad \text{Eq. (1)}$$

Where, A_0 is the absorbance at room temperature (25 ^{o}C).

A_T is the absorbance after baking at T ^{o}C.

A_R is the relative absorbance after baking at T ^{o}C.

4.2.4 Calculation of the intra-molecular interaction of dye aggregates

Intra-molecular interaction of dye aggregates was calculated by Quantum Mechanics (QM) based on Density Functional Theory (DFT). The BLYP functional and DNP basis set embedded in DMOL3 code (Materials Studio v5.0 in Accelrys, USA) was adopted and atomic orbital cut-off distance was set as 4.5 Å.

The degradation enthalpy of single azo dye, ΔH should have been calculated by Eq. (2). However, in this paper, we considered breaking of azo group is the only pathway for the azo dye since azo group is the weakest bond in azo dye. With this premise, since the aggregated and dissociated states of dyes are solid crystalline materials, the rotation and transition of dyes could be left out. And the variation and volume change of the dyes would be ignorable compared with the internal electronic energy (ΔU). However, in recent calculations for phase

change enthalpy, zero-point energy (ZPE) should be considered [26]. Therefore, degradation energy at the *absolute zero* could be defined as a function of the internal energy (U) and zero-point energy as shown in Eq. (3).

$\Delta H = \Delta U + \Delta H_{rot} + \Delta H_{trans} + \Delta H_{vib} + \Delta pV$ ····· Eq. (2)

Where, ΔU is internal energy.

ΔH_{rot} is rotational energy.

ΔH_{trans} is transitional energy.

ΔH_{vib} is vibrational energy.

$\Delta H = \Delta U + \Delta E_{ZPE}$, where ΔE_{ZPE} is zero point energy. ····· Eq. (3)

Aggregates of azo dyes are affected with their strong inter-molecular attraction. In particular, dyes with sodium sulfonate group, such as the prepared dyes have very strong electrostatic attraction as shown in Figure 4.4(b). In order to investigate the variation of intra-molecular interactions for the structurally isomeric dyes, the dissociation enthalpy (ΔH_{dis}) - a bonding dissociation energy for a single dye molecule in dye aggregates, was calculated by Eq. (4).

ΔH_{dis} = ΔU(Aggregated state) - ΔU(Dissociated state) + ΔE_{ZPE} (Aggregated state) - ΔE_{ZPE} (Dissociated state) ····· Eq. (4)

4.3 Results and discussion

4.3.1 Thermogravimetric analysis (TGA) and Differential scanning calorimetry (DSC) of the dyes

Figure 4.1(a) shows TGA curves and denstity values of the prepared water-soluble hydroxyl azo dyes. The degradation temperatures caculated from TGA curves generally increased in proportion to the density values, while they did not have clear melting temperatures [21].

Figure 4.1(b) shows TGA and DSC data of the water-soluble dye **1b**, dye **2b** and the water-insoluble azo dye, which has a corresponding aromatic backbone of dyes **1b** and **2b** . DSC curves of dyes **1b** and **2b** did not demonstrate clear endothermic melting peaks while distinct exthothermic degradation peaks could be seen from their DSC curves. Their degradation temperatures from DSC curves corresponded well to those of TGA curves. On the other hand, the water-insoluble azo dye showed clear endothermic melting peaks in the DSC analysis and had a much lower degradation temperature compared to dye **1b** and dye **2b**. From these results, it could be pressumed that the degradation mechanism of the water-soluble hydroxyl azo dyes differ from that of the water-insoluble azo dye, which is dicussed in chapter 4.3.4.

(a)

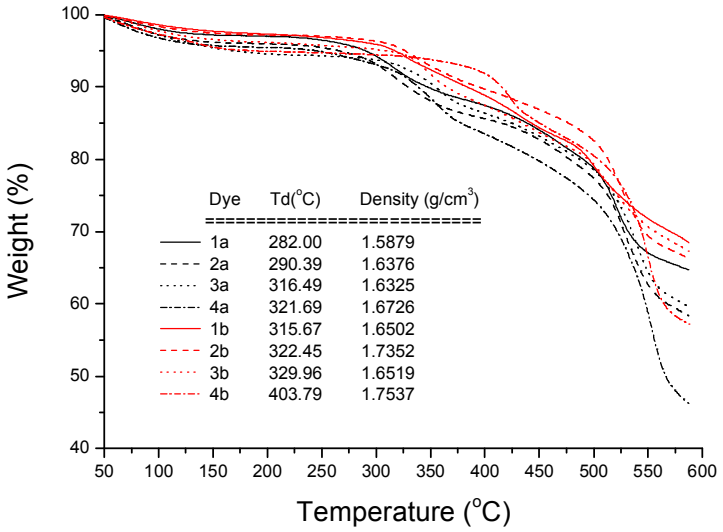

(b)

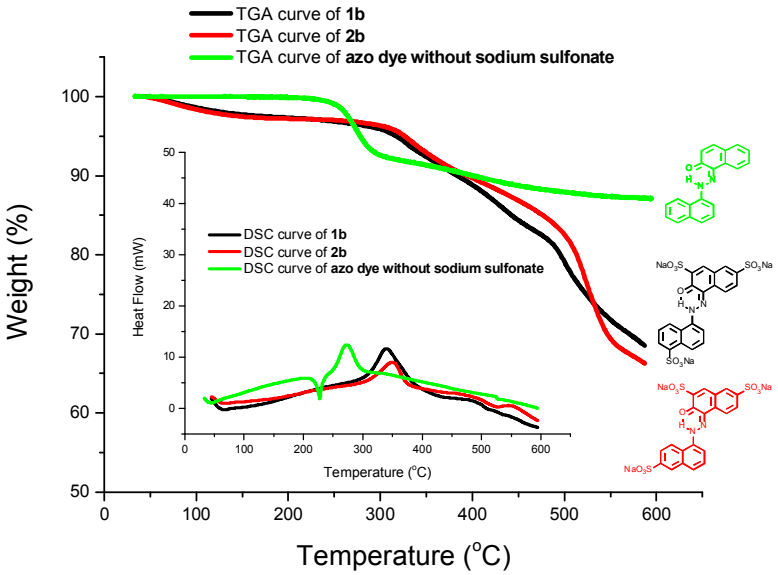

Figure 4.1 TGA[21], DSC and density data of prepared dyes. (The weight loss up to 150 °C is due to the evaporation of H_2O and DMF.)

4.3.2 Crystalline properties of the dye aggregates

In general, the water-insoluble dyes such as the disperse dye show clear melting peaks and regular packing structures [27,28]. However, the prepared water-soluble dyes showed crystalline properties and did not exhibit melting points in the DSC curves. Figure 4.2 shows the crystalline properties of dyes **4a** and **4b.** Both **4a** and **4b** dyes showed unique peaks at 6.3^{o} and 26^{o} of 2θ; thus, they exhibit interplanar spacing whose distance between surfaces is 14 Å and 3.4 Å, respectively. However, it was difficult to obtain more information on the packing structure since the dyes were not in a single crystalline phase. On the other hand, in dye **4b**, an additional peak was formed at 8.4^{o}, resulting from the existance of Na^{+} for multi-ionic interaction [21]. In other words, the additional Na···O=C attraction with adjacent molecules, did generate a new packing parameter correspoding to the 8.4^{o}. This different molecular packing parameter between dye **4a** and **4b** was also shown in dynamic light scattering data, and is discussed in detail in chapter 4.3.3.

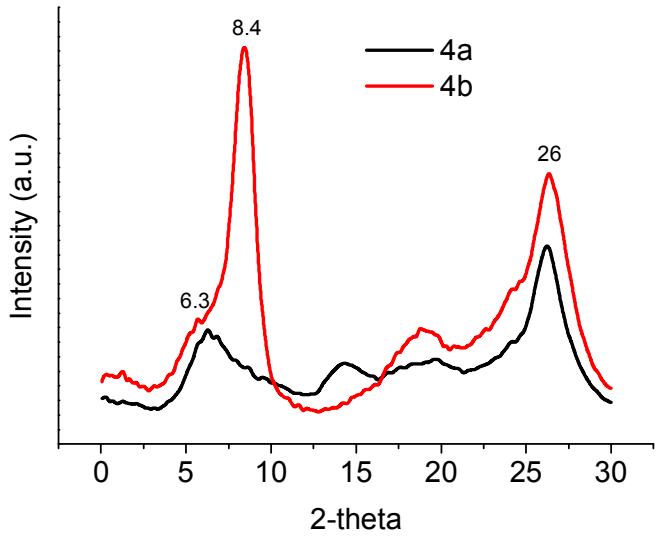

Figure 4.2 XRD data of dyes **4a** and **4b**.

4.3.3 Dynamic Light Scattering (DLS) data of the dye aggregates

Figure 4.3 shows the particle size analysis data of dyes **4a** and **4b**. For the case of dye **4a**, diameters of aggregates were distributed in the range of 30 nm - 100 nm. On the other hand, dye **4b** had binordal distribution at the range of 100 nm - 600 nm. Since the prepared water-soluble dyes are structurally isomeric, the aggregate size of the dyes can be proportial to the inter-molecular interaction of them. Therefore, it can be presumed that the inter-molecular interaction of dye **4b** is stronger than that of dye **4a**. Additionally, the binordal graph of dye **4b** indicates that the dye aggregates are rod-shape particles with a high aspect ratio, since the DLS equipment measures the diameter as it perceives a material as a globular shape [29]. This can also be seen from XRD, considering the fact that 8.4^{o} peak generated from the additional Na···O=C attraction with adjacent molecules shows very high intensity. Thus, it can be inferred that the packing parameter corresponding to the 8.4^{o} plays an important role in making rod-shaped aggregates for dye **4b**.

(a)

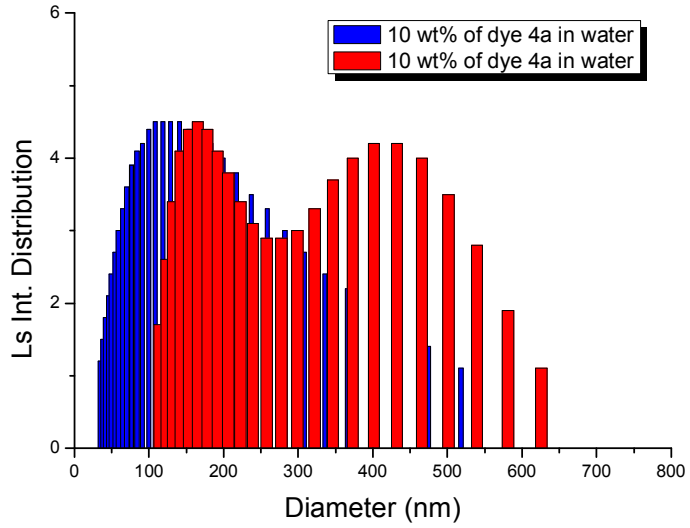

(b)

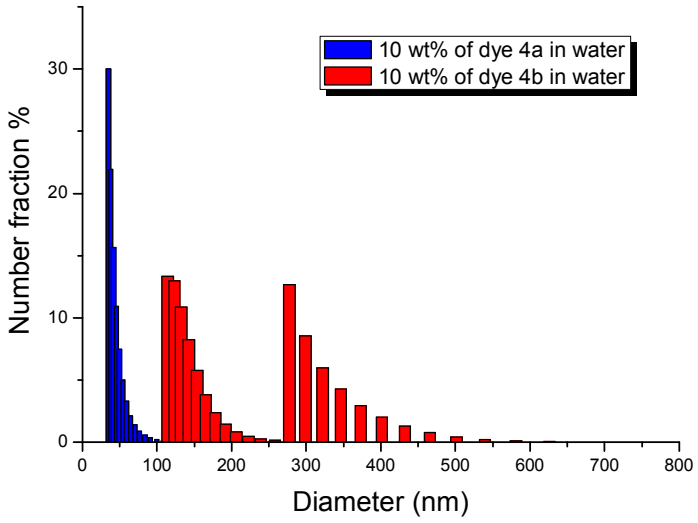

Figure 4.3 Particle size analysis data of dyes **4a** and **4b.**

4.3.4 Thermal decomposition mechanisms of the prepared dyes

As shown in Figure 4.1(b), the degradation temperature of the water-insoluble dye was higher than its melting temperature, and the water-insoluble hydroxyl azo dye rapidly lost its weight beyond the degradation temperature, which is similar to the weight loss of general water-insoluble azo dyes [30,31]. In this case, the dye molecules were presumed to have decomposed simultaneously following the melting of dye aggregates as shown in Figure 4.4(a). That is, since the intra-molecular interaction of the water-insoluble dye is stronger than its inter-molecular interaction, the decomposition of the dye molecules occurs after the melting process.

On the other hand, in case of water-soluble dyes, only degradation peaks were shown and their melting peaks could not be confirmed in the DSC curves (Figure 4.1(b)). Furthermore, their weight losses in the TGA curves occurred gradually beyond the degradation temperatures (280-400 ^{o}C). Therefore, it could be presumed that the thermal decomposition mechanism of the prepared water-soluble dyes differ from that of the water-insoluble azo dye. In regards to that, one might ask how and why the prepared water-soluble dyes would have different decomposition behavior from that of the general water-insoluble dye, and how they could be decomposed in a wide range of degradation temperatures. The answer to this question came from the results of the UV-Vis. spectrophotometry study for the heat treated dyes at various temperatures.

(a)

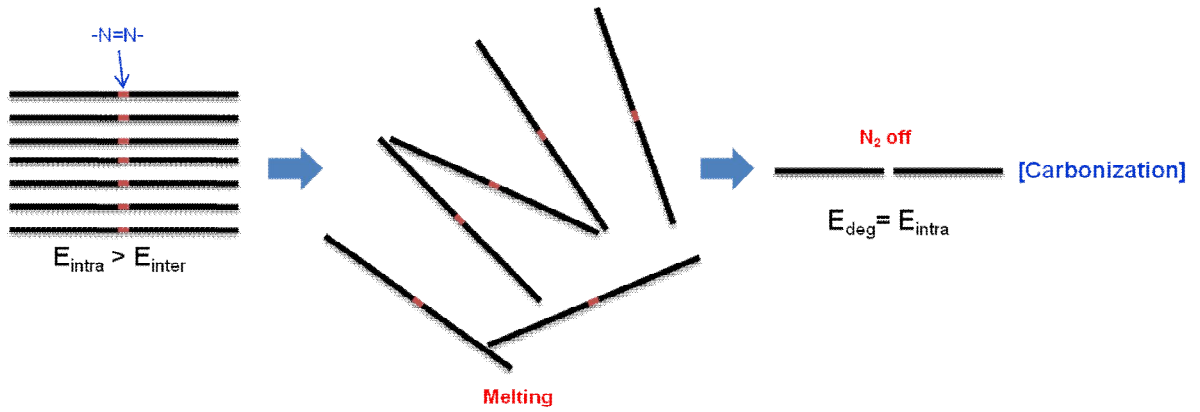

(b)

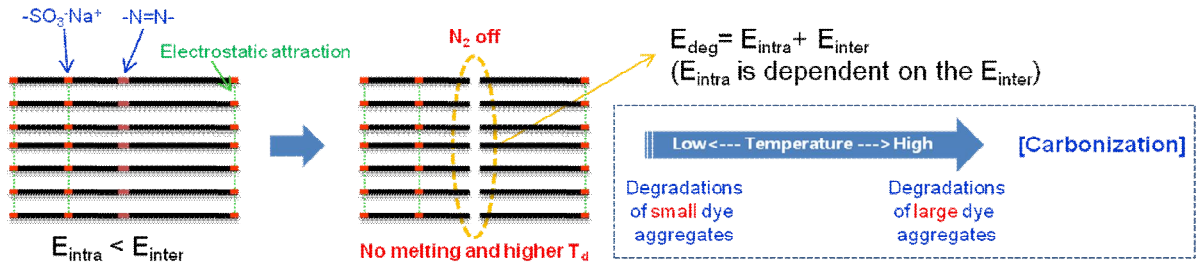

Figure 4.4 Two different decomposition mechanisms of dye molecules.

Figure 4.5 shows the UV-Vis. absorption spectra and color changes of water-insoluble dye and water-soluble dyes **1a** and **4b** in water after baking at various temperatures. As shown in Figure 4.5(a), the water-insoluble dye exhibited rapid color change and absorbance within 250 - 300 ^{o}C, which is corresponds to its TGA data (Figure 4.1(b)). So, it can be concluded that this sharp change resulted from the thermal breakage of the azo group - chromophore of the dye. However, as shown in Figure 4.5(b) and Figure 4.5(c), both of the two water-soluble dyes showed gradual decolorization beyond the degradation temperature even though they had the same aromatic back bone of the water-insoluble dye. Moreover, the azo group of dye **1a** with a lower density dissociated and decolorized more rapidly compared to dye **4b**. For the case of dye **1a** with the lower density, its color strength dropped gradually within 250 - 350 ^{o}C. For the case of dye **4b** with the higher density, its decolorization started from 350 ^{o}C and it became colorless at 450 ^{o}C.

(a)

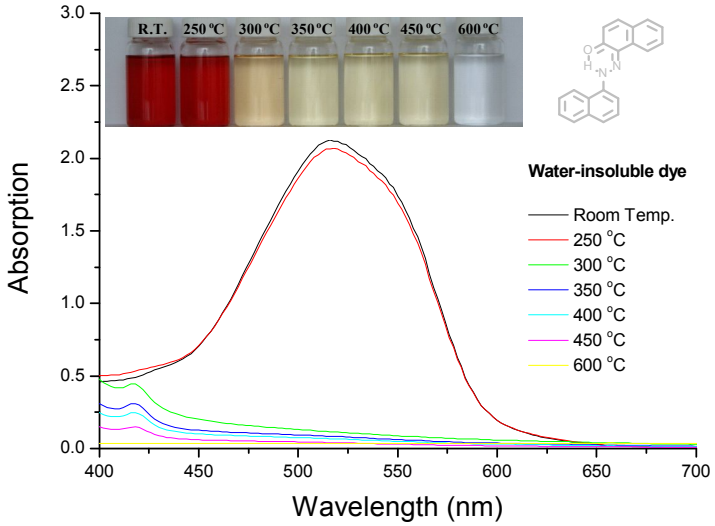
R.T.
250 °C
300 °C
350 °C
400 °C
450 °C
600 °C
Water-insoluble dye
Room Temp.
250 °C
300 °C
350 °C
400 °C
450 °C
600 °C
Absorption
Wavelength (nm)

(b)

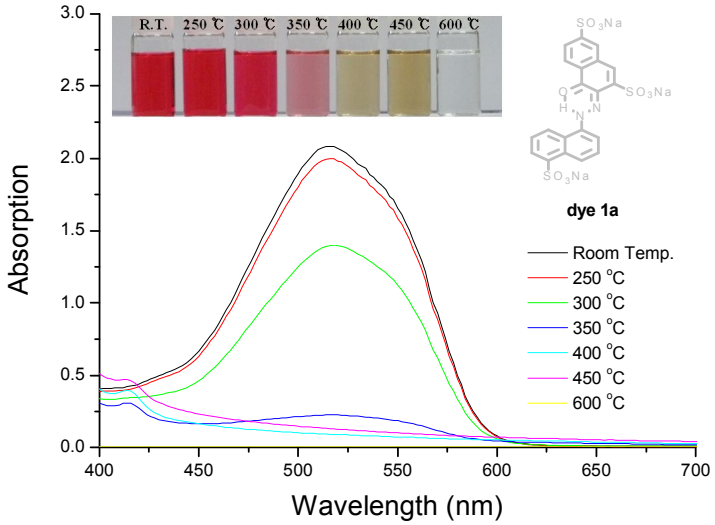
R.T.
250 °C
300 °C
350 °C
400 °C
450 °C
600 °C
dye 1a
Room Temp.
250 °C
300 °C
350 °C
400 °C
450 °C
600 °C
Absorption
Wavelength (nm)

(c)

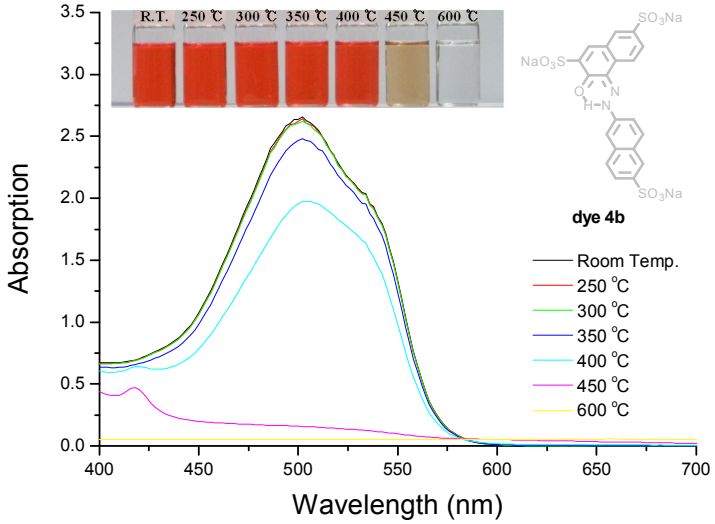

Figure 4.5 The representative UV-Vis absorption spectra and images of color change of water-insoluble dye (a) in cyclohexanone and dyes **1a** (b) and **4b** (c) in H_2O at the various temperatures.

Table 4.1 shows relative absorbance intensity (A_R), which is the representitive residue of chromophore according to the heating temperature. Inter-molecular interactions of the prepared dyes could be proportial to their density since all the dyes studied are structural isomers. As shown in Table 1, the "**b** series" of the dyes showed less degradation of chromophore compared to the "**a** series" of the dyes with lower density and weaker inter-molecular interaction. To examine the relationship of inter-molecular interactions and thermal degradation temperatues of the dyes, their intra-molecular interactions - the bond dissociation enthalpy (ΔH_{dis}) of azo group for the single dye molecule, were calculated as shown in Figure 4.6. It could be seen that as the aggregation number increased, dissociation enthalpy of the dyes decreased. Therefore, it is thought that the decomposition temperatues of the dyes increased by stablization of intra-molecular interaction which was induced by the increase of inter-molecular interaction.

Also, in comparison with ΔH_{dis} at the same aggregation number, the intra-molecular interaction of dye **4b** was more stable than that of dye **4a**. In other words, the induced intra-molecular energy stabilization from the increased inter-molecular interaction was more effective in the "**b** series" of dyes. It is thought that in dyes **1b**-**4b**, multi-ionic interactions resulted from $SO_3^-Na^+$ ionic pairs existing in the *ortho*-position of the carbonyl group could reinforce their intra-molecular interactions [21].

Table 4.1 The relative absorbance (A_R) of dyes according to the heating temperature

Dye	Density (g/cm^3)	λ_{max} [a] (nm)	A_R						
			Baking Temperature						
			25 °C	250 °C	300 °C	350 °C	400 °C	450 °C	600 °C
1a	1.59	518	100	95.77	67.15	10.82	4.38	6.20	0.53
1b	1.65	518	100	98.42	94.01	50.33	15.68	8.55	1.15
2a	1.64	518	100	93.50	91.30	14.37	3.66	5.01	1.53
2b	1.73	518	100	98.91	97.22	74.57	33.69	5.06	0.18
3a	1.63	502	100	94.57	76.52	13.35	2.33	3.34	0.12
3b	1.65	502	100	98.40	95.14	57.52	18.01	8.04	1.13
4a	1.67	502	100	97.63	95.87	29.93	4.21	4.20	0.03
4b	1.75	502	100	99.45	98.61	93.35	74.29	6.00	0.11

[a] Measured in H_2O.

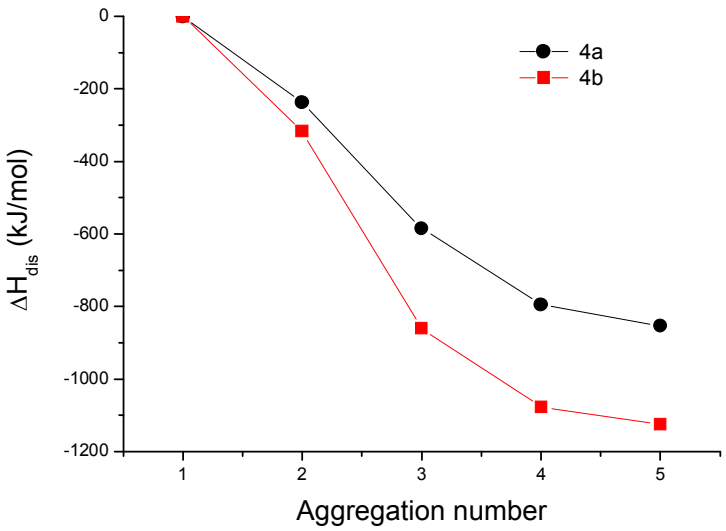

Figure 4.6 Intra-molecular interaction of aggregates of the dyes **4a** and **4b**.

Moreover, Figure 4.6 explains the result that the decomposition temperature of the synthetic water-soluble dye molecules decreased gradually (Figure 4.1). As shown in Figure 4.3, particle sizes of the synthetic water-soluble dyes have broad distribution. Here, the aggregates with larger diameters and higher aggregation numbers, would have stronger inter-molecular interaction and greater stabilized intra-molecular interactions than those with smaller particle sizes. This result could explain that, for the prepared water-soluble dyes, dye aggregates with smaller particle size degraded first and those with larger particle size degraded later. Thus, the thermal degradation of dyes occurred slowly and gradually within the wide-ranged temperature of 250 - 450^{o}C.

This thermal degradation mechanism of water-soluble dyes was presented in Figure 4.4(b). Since the prepared water-soluble dyes have stronger inter-molecular interactions than intra-molecular interactions due to the additional electrostatic attraction of the sodium sulfonate group, they could be decomposed without the melting process even though they exhibited crystalline properties. Besides, intra-molecular interactions of dye molecules could be stabilized when the dyes have stronger inter-molecular interactions (Figure 4.6).

4.4 Conclusion

Structurally isomeric water-soluble hydroxyl azo dyes were synthesized and their thermal properties were evaluated by TGA and DSC. The prepared water-soluble dyes with strong electrostatic inter-molecular interactions decomposed gradually without melting and their degradation temperatures increased in proportion to their inter-molecular interaction. When the prepared water-soluble dyes had higher density – stronger inter-molecular interaction, they exhibited higher degradation temperatures since the dyes with stronger inter-molecular interactions could have stabilized intra-molecular interactions of the dye molecules.

While the thermal stabilities of azo dyes are reported to be weak in general, this research can provide a new molecular design concept for preparing highly heat-resistant azo dyes by improving their inter-molecular interactions.

4.5 References

[1] Gordon P.F, Gregory P. Organic chemistry in colour. Berlin: Springer-Verlag; 1983. p.95-162.

[2] Ferreira J, Santos M.J.L, Matos R, Ferreira O.P, Rubira A.F, Girotto E.M. Structural and electrochromic study of polypyrrole synthesized with azo and anthraquinone dyes. Journal of Electroanalytical Chemistry 2006;591:27-32.

[3] Chernyakovskil F. P, Gribanov V. A. Electrochromism of azo dyes. Journal of Structural Chemistry 1968;9(3):387-391.

[4] Isak Stefan J, Eyring Edward M, Spikes John D, Meekins Patricia A. Direct blue dye

solutions: photo properties. Journal of Photochemistry and Photobiology A: Chemistry 2000;134:77-85.

[5] Salvador Maria A, Reis Lucinda V, Almeida Paulo, Santos Paulo F. Delocalized cationic azo dyes containing a thiazole moiety. Tetrahedron 2008; 64:299-303.

[6] Anithaa, Venugopala Reddy K. R, Vittala Rao K. S. Synthesis and antimicrobial evaluation of metal (II) complexes of a novel bisazo dye 2, 2^1 [benzene-1, 3-diyl di (E) diazene 2, 1-diyl] bis (4-chloroaniline). J. Chem. Pharm. Res. 2011;3(3):511-519.

[7] Yan Li, Brian O. Patrick, David Dolphin. Near-Infrared Absorbing Azo Dyes: Synthesis and X-ray Crystallographic and Spectral Characterization of Monoazopyrroles, Bisazopyrroles, and a Boron-Azopyrrole Complex. J. Org. Chem. 2009;74:5237-5243.

[8] Gregory P. High-Technology Applications of Organic Colorants. New York: Plenum Press; 1991. p.175-205.

[9] Ohya H, Morimoto H. Water based ink composition and image forming method. US 2001/0023652 A1.

[10] Ishizuka T, Hokazono H, Yamanouchi J. Color composition, ink for ink-jet recording and ink-jet recording method. US 6670410 B2.

[11] Koga N, Goto K, Kobayashi N, Aoyama M, Higashiyama S, Fujioka M. Water base ink for ink-jet recording. US 6648463 B2.

[12] Oki Y, Kitamura K, Aoyama T, Uotani N, Takahashi H, Ito Y. Aqueous Ink. US 2002/0050226 A1.

[13] Muruganandham M, Swaminathan M. Solar photocatalytic degradation of a reactive azo dye in TiO_2-suspension. Solar Energy Materials and Solar Cells 2004;81(4): 439-457.

[14] Konstantinou Ioannis K, Albanis Triantafyllos A. TiO_2-assisted photocatalytic degradation of azo dyes in aqueous solution: kinetic and mechanistic investigations: A review. Applied Catalysis B: Environmental 2004;49:1-14.

[15] Millington Keith R, Fincher Keith W, Lee King A. Mordant dyes as sensitisers in dye-sensitised solar cells. Solar Energy Materials and Solar Cells 2007;91(17): 1618-1630.

[16] Ohlsson J, Wolpher H, Hagfeldt A, Grennberg H. New dyes for solar cells based on nanostructured semiconducting metal oxides Synthesis and characterisation of ruthenium(II) complexes with thiol-substituted ligands. Journal of Photochemistry and Photobiology A: Chemistry 2002;148:41-48.

[17] Kim Seok-Soon, Jo Jang, Chun Chaemin, Hong Jae-Chul, Kim Dong-Yu. Hybrid solar cells with ordered TiO_2 nanostructures and MEH-PPV. Journal of Photochemistry and Photobiology A: Chemistry. 2007;188: 364-370.

[18] Song DH, Kim JP. Effect of transition moments and orientational behavior of dichroic dyes on the optical anisotropy of poly(vinyl alcohol) polarizing films. Dyes and Pigments 2009;80:219-225.

[19] Song DH, Yoo HY, Kim JP. Synthesis of stilbene-based azo dyes and application for dichroic materials in poly(vinyl alcohol) polarizing films. Dyes and Pigments 2007;75:727-731.

[20] Chang JB, Hwang JH, Park JS, Kim JP. The effect of dye structure on the dyeing and optical properties of dichroic dyes for PVA polarizing film. Dyes and Pigments 2011;88:366-371.

[21] Kim YD, Cho JH, Park CR, Choi JH, Yoon C, Kim JP. Synthesis, application and investigation of structure–thermal stability relationships of thermally stable water-soluble azo naphthalene dyes for LCD red color filters. Dyes and Pigments 2011;89:1-8.

[22] Kim YD, Kim JP, Kwon OS, Cho IH. The synthesis and application of thermally stable dyes for ink-jet printed LCD color filters. Dyes and Pigments 2009;81:45-52.

[23] Chang CJ, Chang SJ, Shin KC, Pan FL. Improving mechanical properties and chemical resistance of ink-jet printer color filter by using diblock polymeric dispersants. Journal of

Polymer Science: Part B: Polymer Physics 2005;43:3337-3353.

[24] Fierz-David H.E, Blangey L. Fundamental processes of dye chemistry. New York: Interscience; 1949. p. 245-246.

[25] Fierz-David H.E, Blangey L. Fundamental processes of dye chemistry. New York: Interscience; 1949. p. 267-268.

[26] Grev Roger S., Janssen Curtis L., Schaefer Henry F. III. Concerning zero-point vibrational energy corrections to electronic energies. J. Chem. Phys. 1991;95(7):5128-5132.

[27] Nejati K, Rezvani Z, Massoumi B. Syntheses and investigation of thermal properties of copper complexes with azo-containing Schiff-base dyes. Dyes and Pigments 2007;75:45-52.

[28] Park KM, Yoon I, Lee SS, Choi G, Lee JS. X-ray crystal structure of C.I. Disperse Blue 79. Dyes and Pigments 2002;54:155-161.

[29] Sugiyama M, Okazaki H, Koda S. Size and Shape Transformation of TiO2 Nanoparticles by Irradiation of 308-nm Laser Beam. Jpn. J. Appl. Phys. 2002;41:4666-4674.

[30] Castro M.C R, Schellenberg P, Belsley M, Fonseca A.M C, Fernandes S. S.M, Raposo M.M M. Design, synthesis and evaluation of redox, second order nonlinear optical properties and theoretical DFT studies of novel bithiophene azo dyes functionalized with thiadiazole acceptor groups. Dyes and Pigments 2012;95:392-399.

[31] Cui Y, Qian G, Chen L, Wang Z, Wang M. Synthesis and nonlinear optical properties of a series of azo chromophore functionalized alkoxysilanes. Dyes and Pigments 2008;77:217-222.

Summary

Eight thermally stable RGB dyes were synthesized and LCD color filters were fabricated using some of these dyes. Adequate RGB transmittance spectra for color filter could be obtained by the addition of yellow and violet colors compensating dyes.

Since the particle size of dyes is smaller than that of pigments, the prepared dye-based color filter had higher optical performance than the pigment-based color filter while it showed a similar thermal resistance to the pigment-based color filter. Additionally, the synthesized dyes were successfully applied to the ink-jet printing system which would be the new manufacturing technology for LCD color filters. Fabricated ink-jet printed color filter did not differ significantly from pigment-based color filter in terms of its thermal stability.

In order to investigate thermal stability of the water-soluble dyes, eight structurally isomeric water-soluble azo dyes were synthesized and their thermal stabilities were examined. All the prepared dyes showed high degradation temperatures (above 280 ^{o}C), while they did not have clear melting temperatures. This might be caused by the aggregation behavior by the strong intermolecular electrostatic attractions. Red color filters with the prepared azo dyes had absorption maxima between 500 nm and 520 nm. In particular, the optimal color filter was fabricated with dye 4a and commercial yellow dye, which showed 98.9% transmittance and a 62.8% color gamut. Its transmittance and color gamut were improved by 7.03% and 9.6%, respectively, compared to the perylene dye-based red color filter. The degradation temperatures of the prepared dyes varied according to their structure, and the structure-thermal stability relationships were examined using the prepared structurally isomeric dyes. The prepared dyes had similar intra-molecular interactions but their thermal degradation temperatures increased in proportion to their inter-molecular interactions, which could be

represented by their densities. MM calculations of the molecular packing structure of the prepared dyes suggested that the electrostatic attraction, steric hindrance and linearity of the dyes could be changed by the position of the azo linkage and sodium sulfonate groups. When the dyes had multi-ionic interactions and linear structures, they could have dense molecular packing structures. On the other hand, steric hindrance between the neighboring dye molecules disturbed the effective molecular packing. The results of MM calculations of the molecular packing corresponded to those of density analysis. In conclusion, for application of the dyes in LCD color filters, dyes with more compact packing structures may have higher density values and degradation temperatures.

Thermal degradation behavior of thermal stable water-soluble dyes was also investigated. In case of the prepared isomeric azo dyes, when the dyes had higher density – stronger inter-molecular interaction, they exhibited higher degradation temperatures since the dyes with stronger inter-molecular interactions could have stabilized intra-molecular interactions of the dye molecules. And the aggregates with larger diameters and higher aggregation numbers, would have stronger inter-molecular interaction and greater stabilized intra-molecular interactions than those with smaller particle sizes. This result could explain that, for the prepared water-soluble dyes, dye aggregates with smaller particle size degraded first and those with larger particle size degraded later. Therefore, the thermal degradation of dyes occurred slowly and gradually within the wide-ranged temperature of 250 – 450 ^{o}C.

초 록

액정디스플레이(LCD) 컬러필터용 색소재료는 안료와 염료로 구분된다. 안료의경우 용매에 용해되지 않고 분산된 상태로 용매 내에 존재하기 때문에 박막 형성시 50 ~ 100 nm 정도의 평균 입자크기를 가지므로 광산란에 의한 투과도의 저하가 일어난다. 이에 반해, 염료는 용매에 녹은 상태로 존재하기 때문에 박막이 형성된 뒤에 50 nm 이하의 평균 입자크기는 가지며, 광산란이 거의 일어나지 않으므로 높은 투과도를 나타내는 색소재료이다. 그러나, 염료는 우수한 광학 특성을 나타냄에도 불구하고, 낮은 내열성 때문에 LCD 컬러필터용 색소재료로 널리 사용되지 못하였다. 본 연구에서는 높은 열안정을 가지는 4종의 퍼릴렌(perylene) 염료와 4종의 프탈로시아닌(phthalocyanine) 염료를 합성하였다. 그리고 합성한 염료를 사용하여 스핀 코팅법으로 컬러필터를 제조한 뒤 안료분산법으로 제조된 컬러필터와 비교하면서 분광 특성 및 열안정성을 고찰하였다. 염료를 이용한 컬러필터의 경우, 열안정성은 안료를 사용한 컬러필터와 유사하였고 안료보다 작은 입자크기로 인해 광산란이 감소되었으며, 투과도(transmittance)와 색특성(chromaticity)이 안료분산법으로 제조된 컬러필터보다 높았다.

LCD 컬러필터의 공정 단순화를 위해서, 합성한 고내열 수용성 RGB 염료와 상용 수용성 바인더를 사용하여 잉크젯 프린팅법으로 컬러필터를 제조하였다. 잉크젯 프린팅법으로 제조된 컬러필터의 경우, 막두께가 낮게 형성되어 색특성은 스핀 코팅법으로 제조된 컬러필터보다 낮았지만, 열안정성은 스핀 코팅법으로 제조된 컬러필터와 동등 수준이었으므로, 합성한 고내열 수용성 염료가 잉크젯 프린팅법에 의한 컬러필터의 제조에 성공적으로 응용될 수 있음을 본 연구를 통하

여 확인할 수 있었다.

한편, 수용성 염료의 열안정성에 대한 연구는 전무한 상태이다. 따라서, 본 논문에서는 수용성 염료의 열안정성에 대해 실험적이고 체계적인 연구를 수행하였다. 즉, 수용성 염료의 구조와 열안정, 수용성 염료의 열분해 메커니즘을 고찰하기 위해서 8종의 구조이성질체 수용성 아조 염료를 합성하였다. 합성한 염료를 이용한 Red 컬러필터는 98.9%의 높은 투과도와 62.%의 높은 색재현 범위를 보여주었다. 합성한 이성질체 염료의 열적 특성은 열중량분석기(thermogravimetric analysis)와 시차 주사 열량측정법(differential scanning calorimetry)를 이용하여 측정되었다. 염료 구조에 따른 차이는 있었지만 모든 염료들은 280 ℃ 이상의 분해온도를 가지고 있었다.

한편, 수용성 염료의 구조와 열안정성의 관계에 대한 고찰을 위하여, 염료의 내열성(분해온도)은 분자내 결합력과 분자간 결합력이 연관되어 있다고 가정하였고, 양자역학계산(quantum mechanics calculation)을 이용하여 이성질체 염료들의 분자내 결합력을 계산한 결과, 이성질체 염료들의 분자내 결합력은 유사한 수준이었다. 반면에, 이성질체 염료들의 분해온도는 밀도에 비례하여 증가하였다. 이에 대한 고찰을 위해, 분자역학계산(molecular mechanics calculation)을 이용하여 염료 분자간 packing 형상을 시뮬레이션 하였다. 시뮬레이션 결과, 염료 분자 구조적 차이에 의해 정전기적 인력(electrostatic attraction), 입체장애(steric hindrance), 선형성(linearity)의 변화가 발생되고, 이러한 변화가 염료의 packing geometry, 밀도, 분해 온도의 변화를 일으킴을 알 수 있었다.

또한, 수용성 염료의 열분해 메커니즘에 대해서 논하였다. 분자간 강한 정전기적 인력이 존재하는 합성된 이성질체 아조 염료의 경우, 용융과정을 거치지 않

고 서서히 분해되었고, 분자간 결합력에 비례하여 분해 온도가 증가 하였다. 즉, 높은 밀도를 가진 (강한 분자간 인력을 가진) 수용성 염료의 경우, 강한 분자간 인력이 분자내 결합에너지를 안정화 시킬 수 있었기 때문에 분해 온도가 높았다. 그리고, 회합체의 크기가 큰 (회합수가 큰) 염료의 경우 입자 크기가 작은 염료 회합체에 비해서 강한 분자간 인력이 존재하고 분자내 결합에너지의 안정화 정도가 더 크게 나타났다. 이러한 결과는 강한 분자간 인력을 가진 수용성 염료의 열분해는 입자 크기가 작은 것에서 입자크기가 높은 순으로 열분해되는 것을 설명할 수 있었다.

주요어: 액정디스플레이(LCD), 컬러필터(color filter), 안료분산법, 잉크젯 프린팅법, 투과도, 색좌표, 색재현범위, 수용성염료, 내열성, 열분해, 아조 염료, 퍼릴렌 염료, 프탈로시아닌 염료, 분자내 인력, 분자간 인력

학번: 2003-21066

List of Publications

Original Papers

1. **Young Do Kim**, Jae Pil Kim, Oh Sang Kwon, In Hee Cho, "The synthesis and application of thermally stable dyes for ink-jet printed LCD", *Dyes and Pigments*, **2009**, 81, 45.

2. Chun Sakong, **Young Do Kim**, Jae-Hong Choi, Chun Yoon, Jae Pil Kim, "The synthesis of thermally-stable red dyes for LCD color filters and analysis of their aggregation and spectral properties", *Dyes and Pigments*, **2011**, 88, 166.

3. **Young Do Kim**, Jung Hyun Cho, Chong Rae Park, Jae-Hong Choi, Chun Yoon, Jae Pil Kim, "Synthesis, application and investigation of structure-thermal stability relationships of thermally stable water-soluble azo naphthalene dyes for LCD red color filters", *Dyes and Pigments*, **2011**, 89, 1.

4. Jea Uk Lee, **Young Do Kim** (equally contributed), Jea Woong Jo, Jae Pil Kim, Won Ho Jo, "Efficiency enhancement of P3HT/PCBM bulk heterojunction solar cells by attaching zinc phthalocyanine to the chain-end of P3HT", *J. Mater. Chem.*, **2011**, 21, 17209.

5. **Young Do Kim**, Jung Hyun Cho, Chong Rae Park, Jae Pil Kim, "A study on thermal decomposition behavior of some water-soluble azo dyes", *New J. Chem.*, **2013**, To be submitted.

List of Presentations

International

1. **Young Do Kim**, Dong Hyun Song, Jae Pil Kim, “Thermal and Optical Properties of Azo dyes for LCD colorfilters”, AATCC International Conference & Exhibition 2004, September 13-17, **2004**, Palmetto expo center, Greenville, SC, U.S.A.

2. **Young Do Kim**, Dong Hyun Song, Jae Pil Kim, “Thermal and Optical Properties of Dyes for LCD colorfilters", Korea-Japan Joint Forum (KJF) 2004, November 3-6, **2004**, Okinawa Seinenkaikan, Naha, Okinawa, Japan

3. **Young Do Kim**, Dong Hyun Song, Jae Pil Kim, "Thermal and Optical Properties of Azo Dyes for LCD Colorfilter", Korea-Japan Joint Forum (KJF) 2005, October 26-29, **2005**, Yousung Hotel, Daejeon, Korea

4. **Young Do Kim**, Song Se Lee, Jae Pil Kim, Yoon Sik Lee, "Dispersibility enhancement of Cu-phthalocyanine using its derivative surfactants", Pacifichem 2005, Intermational Chemical Congress of Pacific Basin Societies, December 15-20, **2005**, Sheraton Waikiki, Honolulu, Hawaii, U.S.A

5. **Young Do Kim**, Dong Hyun Song, Jung Jin Lee, Chun Sakong, Seong Su Jang, and Jae Pil Kim, “Thermal and optical properties of Azo dyes for LCD colorfilter”, Korea-Japan Joint Forum (KJF) 2006, October 2-5, **2006**, Niigata, Japan

6. Chun Sakong, **Young Do Kim**, Jae Pil Kim, “Synthesis application of thermally stable red dyes for LCD colorfilter; Influence of dye structures on the aggregation property in the film state”, International Meeting on Information Display/International Display Manufacturing Conference/ASIA DISPLAY, **2008**, October 13-17, KINTEX, Ilsan, Korea

Domestic

1. **김영도**, 송동현, 김재필, "Thermal and Optical Properties of Azo Dyes for LCDcolorfilters", 2004 추계 한국고분자학회, October 8-9, **2004**, 대구 GS프라자, 대구

2. **김영도**, 송동현, 김재필, "Synthesis and Charaterizaion of High Durable Azo Dyes for LCD colorfilter", 2005 추계 한국고분자학회, October 13-14, **2005**, 제주국제컨벤션센터, 제주

3. **김영도**, 이송세, 김재필, 이윤식, “Synthesis and Characterization of novel Cu-phthalocyanine derivative surfactants” 2006 추계 한국공업화학회, November 10-11, **2006**, 경희대학교, 수원

4. 사공천, 김세훈, **김영도**, 김재필, “Synthesis and Characterizations of New Water-Soluble Phthalocyanine-Based Blue Colorants for LCD Colorfilter”, **2007** 추계 한국고분자학회, October 11-12, 2007, KINTEX, 일산

5. **김영도**, 송동현, 이정진, 김재필, “Thermal and Spectural Properties of Azo Dyes for LCD Colorfilter”, **2007** 추계 한국고분자학회, October 11-12, 2007, KINTEX, 일산

6. 이제욱, **김영도**, 김재필, 조원호, “Synthesis ans Photophysical properties of a Novel Diblock Copolymer Comprising of Poly (3-hexylthiophene)Block and Zinc Phthalocyanine-Containing Block”, 2009 춘계 한국고분자학회, April 9-10, **2009**, 대전컨벤션센터, 대전

7. **김영도**, 김재필, “The synthesis and application of thermally stable dyes for LCD color”, 2009 춘계 한국고분자학회, April 9-10, **2009**, 대전컨벤션센터, 대전

List of Patents

1. 송동현, **김영도**, 김재필, “네온 발광 및 근적외선을 동시에 흡수할 수 있는 PDP 필터용 색소 화합물 (Dyes for PDP filter absorbable neon and near IR radiation at the same time)”, Korea patent [등록번호: 100764589 (2007.10.01)].

2. **김영도**, 김재필, 권오상, 조인희, 노은미, 갈승훈, “페릴렌 단위를 포함하는 수용성 적색염료 화합물, 그 제조방법, 이를 포함한 잉크 조성물 및 컬러필터 (Red dyes compound containing water soluble perylene and ink composition, color filter, method of producing the same)”, Korea patent [등록번호: 101040729 (2011.06.03)].

3. **김영도**, 이정진, 박승희, “적외선 위장 기능을 갖는 금속-프탈로시아닌계 화합물 및 이를 포함하는 염료 조성물 (Metal-phthalocyanine-based compounds having infrared reflectance function and a dye composition comprising the same)”, Korea patent [출원번호: 10-2011-0089835 (2011.09.05)].